HHS Public Access

Author manuscript

Nat Metab. Author manuscript; available in PMC 2022 June 27.

Published in final edited form as:

Nat Metab. 2021 November ; 3(11): 1569–1584. doi:10.1038/s42255-021-00488-3.

Loss of *Hilnc* prevents the development of diet-induced hepatic steatosis through IGF2BP2

Yiao Jiang[1,10],
Jiayin Peng[1,10],
Jiawen Song[1],
Juan He[1],
Man Jiang[4],
Jia Wang[1],
Liya Ma[1],
Yuang Wang[1],
Moubin Lin[6],
Hailong Wu[7],
Zhao Zhang[8,9],
Dong Gao[1,2,3],
Yun Zhao[1,4,5,11,*]

[1]The State Key Laboratory of Cell Biology, Shanghai Institute of Biochemistry and Cell Biology, Center for Excellence in Molecular Cell Science, Chinese Academy of Sciences; University of Chinese Academy of Sciences, Chinese Academy of Sciences, Shanghai 200031, China

[2]Shanghai Key Laboratory of Molecular Andrology, CAS Center for Excellence in Molecular Cell Science, Shanghai Institute of Biochemistry and Cell Biology, Chinese Academy of Sciences, Shanghai 200031, China.

[3]Institute for Stem Cell and Regeneration, Chinese Academy of Sciences, Beijing 100101, China

[4]School of Life Science and Technology, ShanghaiTech University, Shanghai 201210, China

[5]School of Life Science, Hangzhou Institute for Advanced Study, University of Chinese Academy of Sciences, Hangzhou 310024, China

[6]Department of General Surgery, Yangpu Hospital, Tongji University School of Medicine, Shanghai, 200090, P. R. China

[*]**MATERIALS & CORRESPONDENCE:** Correspondence and requests for materials should be addressed to Y.Z. (yunzhao@sibcb.ac.cn).

[10]These authors contributed equally

[11]Lead Contact

AUTHOR CONTRIBUTIONS

Y.Z. conceived and designed the experimental approach. Y.A.J. performed most experiments. J.Y.P. contributed to the mice experiments and statistical analysis. J.W.S., M.J., J.W., L.Y.M., Y.A.W., and J.H. helped the experiments and provided technical support. M.B.L., Z.Z., H.L.W. and D.G. helped to design experiments and provided useful discussion. Y.A.J. and Y.Z. wrote the manuscript.

COMPETING INTERESTS

The authors have no competing interests to declare.

[7]Shanghai Key Laboratory for Molecular Imaging, Collaborative Research Center, Shanghai University of Medicine & Health Science, Shanghai, 201318, P. R. China.

[8]Center for the Genetics of Host Defense, University of Texas Southwestern Medical Center, Dallas, TX 75390, USA.

[9]Division of Endocrinology, Department of Internal Medicine, University of Texas Southwestern Medical Center, Dallas, TX 75390, USA.

Abstract

The Hedgehog (Hh) signaling pathway plays a critical role in regulating liver lipid metabolism and related diseases. However, the mechanism of the Hh signaling pathway in regulating liver lipid metabolism is poorly understood. Here, we found that the Hh signaling pathway directly regulates an undefined lncRNA (*Hilnc*, **H**edgehog signaling-**i**nduced **l**ong noncoding RNA). Mutation of the Gli binding sites in the *Hilnc* promoter region ($Hilnc^{BM/BM}$) dramatically decreased the expression of *Hilnc in vitro* and *in vivo*. $Hilnc^{BM/BM}$ and *Hilnc*-knockout mice were resistant to diet-induced obesity and hepatic steatosis through attenuation of the PPAR signaling pathway. *Hilnc* directly interacted with IGF2BP2 to regulate the mRNA stability of *Pparγ*. Furthermore, we identified the potential functional human homolog of *Hilnc*, *h-Hilnc*, which has the similar function of *Hilnc* in lipid metabolism. These findings uncover a critical role of the Hh-*Hilnc*-IGF2BP2 axis in lipid metabolism and suggest a potential therapeutic target of diet-induced hepatic steatosis.

Keywords

Hh signaling; LncRNA; *Hilnc* ; Gli; IGF2BP2; Diet-induced obesity; Lipid metabolism

INTRODUCTION

The Hedgehog (Hh) signaling pathway is an evolutionarily conserved pathway controlling tissue development and homeostasis. The core components of the Hh signaling pathway include Hh ligands (Sonic, Indian, or Desert Hedgehog), the Patched transmembrane receptors (PTCH) 1 and 2, the G protein-coupled-receptor-like protein Smoothened (SMO), and the glioma-associated oncoproteins Gli1, Gli2, and Gli3 (Rubin and de Sauvage, 2006). In normal adult tissues, the Hh signaling pathway is mainly quiescent, except when tissue maintenance is required (Kasper et al., 2009). Activation of the Hh signaling pathway is initiated by external Hh ligand morphogens. Hh ligands bind to the receptor PTCH1 to relieve its inhibition of SMO, a seven-pass transmembrane protein, resulting in transcriptional activation by Gli family proteins (Ingham and McMahon, 2001). Gli family proteins are key transcription factors in the Hh signaling pathway, and upregulation of their activity is one of the most important markers of Hh signaling pathway activation. They regulate the transcription of downstream genes by directly binding to the consensus Gli binding site, GACCACCCA (Hallikas et al., 2006; Kinzler and Vogelstein, 1990).

Hh signaling regulates multiple cellular processes, including important metabolic programs. It specifically blocks the adipogenesis of white adipose tissue (WAT), but not brown adipose tissue (BAT) (Claussnitzer et al., 2015; Pospisilik et al., 2010; Suh et al., 2006). This

biological effect is sensitive to the inflammatory state (Todoric et al., 2011) and represents one of the few known signaling nodes that are capable of differentially regulating brown versus white adipocyte differentiation (Pospisilik et al., 2010). Hh signaling drives Warburg-like metabolism in muscle and brown fat (Teperino et al., 2012) and has recently been described as a novel regulator of liver lipid metabolism (El-Agroudy et al., 2016; Gao et al., 2018; Guillen-Sacoto et al., 2017; Marbach-Breitruck et al., 2019). Activation of the Hh signaling pathway has been observed in both human and mouse with nonalcoholic fatty liver disease (NAFLD) (Guy et al., 2012; Kwon et al., 2016; Swiderska-Syn et al., 2013); Inhibition of Hh signaling pathway reverses myofibroblasts to a quiescent phenotype, thus reducing the hepatic myofibroblast content and attenuating fibrosis (Choi et al., 2011; El-Agroudy et al., 2016). Dysfunctions of the Hh signaling pathway play an important role in hepatic steatosis and beyond (Matz-Soja et al., 2016).

Long noncoding RNAs (lncRNAs) are defined as transcripts longer than 200 nucleotides that are 5'-capped and 3'-polyadenylated, similar to most mRNAs, and lack coding potential. Genome-scale analyses using chromatin immunoprecipitation (ChIP) and gene expression profiling have revealed many putative Gli target genes (Lee et al., 2010; Vokes et al., 2007; Vokes et al., 2008), and most of the protein-coding genes regulated by Hh signaling have been extensively studied. However, whether Hh signaling regulates lncRNAs remains largely unknown. Recently, a large number of lncRNAs have been identified in humans and other mammals (Morris and Mattick, 2014), and dysregulated lncRNA expression profiles are involved in the pathogenesis of many diseases (Geisler and Coller, 2013; Huarte, 2015; Lee, 2012; Prasanth and Spector, 2007; Quinn and Chang, 2016). LncRNAs function in a wide range of processes and regulate the expression of either nearby genes (acting in *cis* in the nucleus) or genes elsewhere in cells (acting in *trans* in the nucleus or cytoplasm) by diverse mechanisms, including recruiting transcription factors or chromatin-modifying complexes to their DNA targets, directly interacting with RNA-binding proteins (RBPs) and regulating their activities, altering RNA processing events, and serving as precursors to small RNAs (Chen, 2016; Mercer et al., 2009; Ponting et al., 2009; Rinn and Chang, 2012). To date, there are very few Hh signaling pathway-related lncRNAs with functional annotations. Some Hh signaling pathway related lncRNAs including H19, BCAR4, lncRNA-Hh, LncHDAC2, XIST, and lncRNA-cCSC1 have been shown to function through Hh signaling (Chan et al., 2014; Del Rosario et al., 2017; Lin et al., 2020; Wu et al., 2019; Xing et al., 2014; Zhou et al., 2020; Zhou et al., 2016). However, the function and mode of action of most Hh signaling-regulated lncRNAs have yet to be elucidated.

In this study, we focused on a previously uncharacterized lncRNA that we named *Hilnc*. We showed that *Hilnc* is directly regulated by Hh signaling through Gli *in vitro* and *in vivo*. *In vivo* depletion of *Hilnc* conferred resistance to diet-induced obesity and liver steatosis in mice. Mechanistically, we demonstrated that *Hilnc* binds to the RNA-binding protein IGF2BP2 to regulate the peroxisome proliferator-activated receptor (PPAR) signaling pathway and plays an important physiological role in mammalian hepatic steatosis. Furthermore, the potential functional human homolog of *Hilnc*, *h-Hilnc*, was identified and it has the similar function of *Hilnc* in lipid metabolism.

RESULTS

Identification of a novel lncRNA, *Gm16364* (*Hilnc*), that is directly induced by Hh signaling

To identify lncRNAs that are regulated by Hh signaling, we activated Hh signaling by treating NIH-3T3 cells with SAG (an SMO agonist) and SHH (Sonic Hedgehog). Then, we performed deep RNA-seq of SAG/SHH-treated and untreated NIH-3T3 cells and identified previously unannotated lncRNAs as well as lncRNAs that were previously annotated in GENCODE and Ensembl. To identify lncRNAs that were reliably expressed in NIH-3T3 cells, we excluded lncRNAs that had very low basal levels.. To identify the lncRNA(s) induced by Hh signaling, we focused on the differentially expressed lncRNAs, especially those upregulated in both SAG- and SHH-treated NIH-3T3 cells (Figure 1A). We identified 29 lncRNAs with more than twofold changes and stable expression in NIH-3T3 cells after treatment with both SAG and SHH (Figures 1B and 1C, Supplementary Table 1). To further identify the direct targets of Hh signaling, we searched for conserved Gli binding sites (GACCACCCA) near the transcription start site (TSS) (±1.5 kb) of the upregulated lncRNAs. Among these transcripts, we noted a novel and poorly characterized lncRNA, annotated as *Gm16364*, which has a conserved Gli binding site in its promoter region (Figures 1C and 1G). We named this lncRNA ***H****edgehog signaling-****i****nduced* ***l****ong* ***n****on****c****oding RNA* (*Hilnc*).

LncRNAs are a newly emerging class of RNAs, and their status as noncoding transcripts in genome annotations requires independent validation. We then determined by rapid amplification of cDNA ends (3’- and 5’-RACE) that *Hilnc* is a 779-nucleotide transcript comprising three exons, consistent with our RNA-seq analysis in NIH-3T3 cells (Figure S1A). We also detected a longer isoform (2,133 bp, isoform 2) that represented only a minor fraction of the total transcripts in NIH-3T3 cells, as determined by quantitative RT-PCR (qPCR) (Figures S1A and S1B). *Hilnc* located in chr10: 39432067–39489678 in the mouse genome (Figure S1C), the whole sequences of the two isoforms were showed in Figure S1D. Cell fractionation followed by qPCR showed that most of the spliced *Hilnc* transcript resides in the cytoplasm (Figure S1E). We then analyzed the protein coding potential of *Hilnc* by two widely employed algorithms, which both indicated that *Hilnc* lacks any coding capacity (Experimental Procedures). In addition, none of the predicted short open reading frames (ORFs) in *Hilnc* matched any known proteins or functional protein motifs in current proteome databases, further suggesting that *Hilnc* is a noncoding transcript.

To confirm the regulation of *Hilnc* by the Hh signaling pathway, we treated NIH-3T3 cells with two different Hh signaling activators (SAG/SHH). qPCR and RNA fluorescence in situ hybridization (FISH) assays showed that treatment with both SAG and SHH upregulated *Hilnc* expression in NIH-3T3 cells, and *Hilnc* was mainly distributed in the cytoplasm (Figures 1D and 1E). To investigate whether the Hh signaling pathway regulates *Hilnc* through its downstream transcription factor Gli, we used SAG and GANT61 together to treat NIH-3T3 cells. GANT61 is known to directly block the binding of Gli to DNA and Gli-mediated transcription (Lauth et al., 2007). We found that the expression of *Hilnc* was inhibited dramatically by GANT61, even under pathway activation by SAG (Figure 1F), suggesting that the Hh signaling pathway regulates *Hilnc* through Gli. To analyze

whether the Gli binding site in the *Hilnc* promoter region is involved in Gli-mediated *Hilnc* expression, we generated three luciferase reporter constructs containing either wild-type (WT), mutant or deleted Gli binding sites (Figure 1G). Luciferase reporter assays showed that overexpression of Gli1 or Gli2 resulted in a significant increase in luciferase activity in the construct with WT Gli binding sites but failed to induce luciferase activity in constructs with mutant or deleted Gli binding sites (Figure 1H). We also found that Gli1 could increase luciferase activity in the WT background in a dose-dependent manner (Figure S1F). This suggested that *Hilnc* expression might be directly regulated by Gli. To further examine whether Gli1 and Gli2 were directly involved in the transcriptional regulation of *Hilnc*, we overexpressed Flag-tagged Gli1 or Gli2 in NIH-3T3 cells and performed a ChIP assay with an anti-Flag antibody, followed by qPCR. We found enrichment of Gli1 and Gli2 at the *Hilnc* locus in NIH-3T3 cells (Figure 1I). In addition, we utilized CRISPR-Cas9 (Ran et al., 2013) to generate a genetically modified NIH-3T3 cell line, in which the Gli binding site in the *Hilnc* promoter region was randomly mutated (3T3-BM, the binding site mutation). As shown in Figure 1J, SAG treatment induced Gli1 expression but failed to induce *Hilnc* expression in 3T3-BM cells. These data suggest that Gli1 and Gli2 activate the transcription of *Hilnc* by interacting directly with the Gli binding site of the *Hilnc* promoter region. *Hilnc* is a lncRNA that is induced by Hh signaling and directly by Gli.

Gli1 directly regulates the expression of *Hilnc in vivo*

To determine the biological functions of *Hilnc*, we next detected its expression in different mouse tissues. The results showed that *Hilnc* basically existed as isoform 1 (Figure 2A), which was consistent with the result in NIH-3T3 cells (Figure S1B). Interestingly, *Hilnc* was highly expressed in key metabolic organs, such as muscle, adipose tissues and liver (Figure 2A), indicating that *Hilnc* might be potentially involved in systemic metabolism. Previous studies have shown that the Hh signaling pathway is activated in both humans and mice with NAFLD, that the levels of Shh are correlated with the severity of NAFLD and that Shh is induced in subcutaneous adipose tissue from obese mice (Guy et al., 2012; Kwon et al., 2016; Swiderska-Syn et al., 2013; Yao et al., 2019a). Therefore, *Hilnc* might also be induced in these metabolic processes. To further investigate this possibility, we fed mice a high-fat diet (HFD). Consistent with previous studies (Kwon et al., 2016; Yao et al., 2019a), Hh signaling activation, as evidenced by *Gli1* and *Ptch1* upregulation, was observed in the liver and white fat tissues but not in the brown fat and muscle of mice fed a HFD (Figure 2B, Figure S2). Moreover, upregulation of *Hilnc* was detectable in the corresponding tissues with Hh signaling activation (Figure 2B, Figure S2B). This synchronous change suggests that *Hilnc* might participate in Hh signaling-regulated metabolic homeostasis.

To further investigate the role of *Hilnc* and the regulation of *Hilnc* by Hh signaling *in vivo*, we generated *Hilnc*-knockout mice ($Hilnc^{-/-}$) and *Hilnc* mutant mice in which the Gli binding site in the *Hilnc* promoter region was randomly mutated ($Hilnc^{BM/BM}$) (Figures 1G and 2C, Figure S3A). Compared to that in WT mice, *Hilnc* expression in mouse embryonic fibroblast (MEF) cells and mouse tissues, such as liver and adipose tissue, was completely eliminated or significantly reduced in $Hilnc^{-/-}$ or $Hilnc^{BM/BM}$ mice, respectively (Figure 2D, Figures S3B–S3E), while there was no significant difference in *Gli1* expression levels among WT, $Hilnc^{-/-}$ and $Hilnc^{BM/BM}$ mice. This finding strongly suggests that the binding

of Gli to the *Hilnc* promoter is critical to maintain homeostatic expression of *Hilnc*. In addition, no hepatic induction of *Hilnc* was observed in $Hilnc^{BM/BM}$ mice after HFD feeding (Figure 2E), although the expression of both *Gli1* and *Ptch1* was upregulated. These findings indicate that Gli binding to the *Hilnc* promoter is responsible for basic or inducible *Hilnc* expression under either physiological or pathological conditions.

$Hilnc^{BM/BM}$ and $Hilnc^{-/-}$ mice are both resistant to diet-induced obesity

$Hilnc^{BM/BM}$ and $Hilnc^{-/-}$ mice were born at the expected Mendelian ratio, appeared normal after birth, survived without difficulty, and were similar in weight to WT mice (Figures S3F and S3G). On a normal chow diet (NCD), the $Hilnc^{BM/BM}$ and $Hilnc^{-/-}$ mice gained the same amount of weight as their WT littermates (Figure 2F, Figure S3H). However, on a HFD, the weight gain in $Hilnc^{BM/BM}$ mice was significantly retarded compared to that in their WT littermates (Figures 2F and 2G). The same trend was observed in $Hilnc^{-/-}$ mice (Figures S3H and S3I). Thus, the $Hilnc^{BM/BM}$ and $Hilnc^{-/-}$ mice were relatively resistant to HFD-induced obesity. All these results suggest that *Hilnc* plays an important role in regulating HFD-induced obesity. Since we did not observe indistinguishable differences between $Hilnc^{BM/BM}$ and $Hilnc^{-/-}$ mice and since $Hilnc^{BM/BM}$ might further reflect the regulation of *Hilnc* by Hh signaling, we mainly employed $Hilnc^{BM/BM}$ mice to perform the following experiments.

To further investigate the role of *Hilnc* in HFD-induced obesity, intraperitoneal glucose tolerance tests and insulin tolerance tests were performed on 12-week-old mice fed a NCD or HFD for 6 weeks. Under NCD conditions, no notable difference was observed between WT and $Hilnc^{BM/BM}$ mice (Figures S3J and S3K). Under HFD conditions, the $Hilnc^{BM/BM}$ mice exhibited consistently lower blood glucose values after intraperitoneal injection of glucose or insulin (Figures 2H and 2I). These data indicate that $Hilnc^{BM/BM}$ mice are resistant to HFD-induced obesity and exhibit glucose tolerance and insulin sensitivity.

$Hilnc^{BM/BM}$ mice exhibit increased energy expenditure but normal food intake, fat absorption, and physical activity

We next sought to define the basis for the greatly diminished fat deposition in the $Hilnc^{BM/BM}$ mice maintained on the HFD. Food intake was measured on a NCD and HFD, respectively. No differences were observed in food intake between the WT and $Hilnc^{BM/BM}$ mice (Figure S4A). The fecal weight and fecal triglyceride (TG) level were measured on a HFD in 14-week-old mice, and there were no differences between the WT and $Hilnc^{BM/BM}$ mice (Figures S4B and S4C). Thus, differential accumulation of fat mass between WT and $Hilnc^{BM/BM}$ mice on a HFD occurs in the absence of measurable differences in food intake per mouse (on either diet) and in the absence of fat absorption. Physical activity was measured on a NCD and HFD, and there was no difference between the WT and $Hilnc^{BM/BM}$ mice (Figure S4D). The respiratory exchange ratio and energy expenditure were estimated using indirect calorimetry. Regardless of whether they were fed with the NCD or HFD, adult mice showed similar oxygen consumption and carbon dioxide production in both genotypes (Figure S4E). Likewise, there were no significant differences in energy expenditure on the NCD between WT and $Hilnc^{BM/BM}$ mice (Figure S4F). However, on the HFD, indirect calorimetric analysis revealed an increase in energy

expenditure corrected for total body weight in *Hilnc*$^{BM/BM}$ mice (Figure S4F). These findings suggest that resistance to HFD-induced obesity may be related to enhanced energy expenditure in *Hilnc*$^{BM/BM}$ mice.

Hilnc$^{BM/BM}$ and *Hilnc*$^{-/-}$ mice are both resistant to fatty liver after HFD

We then examined the histology of some tissues that are important to the regulation of nutrient metabolism. At the histological level, the skeletal muscle and pancreas of WT and *Hilnc*$^{BM/BM}$ mice were indistinguishable on the HFD (data not shown). Compared with WT mice, *Hilnc*$^{BM/BM}$ mice had less white fat in the groin on the HFD (Figure 3A). H&E staining of WAT showed that there was no difference in adipocyte size between *Hilnc*$^{BM/BM}$ and WT mice on the NCD (Figure 3B, left panel). On the HFD, however, the adipocyte size in the WAT of *Hilnc*$^{BM/BM}$ mice was smaller (Figure 3B, right panel). The most striking difference in histological appearance between WT and *Hilnc*$^{BM/BM}$ mice was found in the livers of mice fed a HFD (Figure 3C, left panel). Although the liver mass was comparable in the NCD-fed *Hilnc*$^{BM/BM}$ mice and WT controls (Figure 3C, right panel), HFD-fed WT mice showed a marked increase in liver mass compared with HFD-fed *Hilnc*$^{BM/BM}$ mice (Figure 3C). Moreover, H&E staining, oil red O staining and total TG measurement of liver tissues showed no difference in NCD-fed mice but significantly reduced fat deposits in HFD-fed *Hilnc*$^{BM/BM}$ mice compared to WT mice (Figures 3D–3F). As expected, reduced fat deposits were also observed in the WAT and liver tissue of *Hilnc*$^{-/-}$ mice compared to those of WT mice (Figures S3L and S3M). Then we evaluated whether the genetic disruption of *Hilnc* influences hepatic de novo lipogenesis (DNL) activity. As shown in Figure 3G, hepatic DNL activity in *Hilnc*$^{BM/BM}$ mice is lower than WT mice. These data indicate that *Hilnc*$^{BM/BM}$ and *Hilnc*$^{-/-}$ mice are resistant to HFD-induced hepatomegaly and that *Hilnc* may play an important role in hepatic steatosis under HFD conditions.

Lack of *Hilnc* decreases lipid accumulation in primary hepatocytes and prevents diet-induced hepatic steatosis

As the liver is the core organ of energy metabolism and Hh signaling has recently been reported to participate in liver metabolism (Gao et al., 2018; Marbach-Breitruck et al., 2019; Matz-Soja et al., 2016), we mainly focused specifically on the function of *Hilnc* in the liver. Compared to those from WT mice, primary hepatocytes isolated from *Hilnc*$^{BM/BM}$ mice showed lower lipid accumulation after treatment with 0.5 mM oleic acid (OA), as determined by oil red O staining and by quantifying the total TG level (Figures 4A and 4B). A methionine and choline-deficient L-amino acid diet (MCD) is another diet, in addition to a HFD, that can directly induce hepatic steatosis in the liver. *Hilnc*$^{BM/BM}$ mice maintained on a MCD for a month were similar in weight to WT mice (Figure 4C) and showed less fat in the liver (Figures 4D and 4E).

Adeno-associated virus 8 (AAV-8) has high affinities for hepatocytes and can transduce up to 90–95% of hepatocytes in the mouse liver following intraportal vein injection. To investigate the role of hepatic *Hilnc* in HFD-induced liver steatosis, we generated hepatocyte-specific *Hilnc*-knockdown mice by administration of sh-*Hilnc*-AAV-8, which carries small hairpin RNA targeting *Hilnc,* into WT mice followed by 10 weeks of HFD feeding (Figure 4F). ZsGreen staining and qPCR showed high transduction efficiency and

successful knockdown of endogenous *Hilnc* in the liver (Figures 4G and 4H). There were no significant differences in body weight, glucose tolerance and energy expenditure between *Hilnc*-knockdown mice and WT mice feeding with HFD for 10 weeks (Figures S5A–S5C). However, knockdown of hepatic *Hilnc* prevented hepatic steatosis, as determined by H&E staining, oil red O staining and hepatic TG analysis (Figures 4H and 4I). In addition, primary hepatocytes isolated from hepatic *Hilnc*-knockdown mice also showed decreased lipid accumulation after OA treatment (Figures 4J and 4K). These results indicate that hepatic *Hilnc* influences lipid accumulation in hepatocytes and diet-induced hepatic steatosis.

Hilnc overexpression in the liver of *Hilnc*$^{-/-}$ mice resulted in increased lipid accumulation

To further determine the functional significance of *Hilnc* in fatty liver *in vivo*, we overexpressed *Hilnc* in the liver by injecting AAV8-*Hilnc* (O/E-Hilnc) into *Hilnc*$^{-/-}$ mice via tail veins followed by 12 weeks of HFD feeding (Figure 5A). Ectopic expression of hepatic *Hilnc* was verified by ZsGreen staining and qPCR (Figures 5B and 5C). No significant differences were observed in body weight, glucose tolerance and energy expenditure between *Hilnc*$^{-/-}$ (AAV-Control) and *Hilnc*$^{-/-}$ (O/E-*Hilnc*) mice feeding with HFD for 10 weeks (Figures S5D–S5F). However, on a HFD, *Hilnc*$^{-/-}$ mice with restored *Hilnc* expression showed higher liver mass and liver TG levels than *Hilnc*$^{-/-}$ mice injected with AAV8-GFP (AAV-Control) (Figures 5D and 5E). Consistent with this notion, H&E staining and oil red O staining of the livers from WT, *Hilnc*$^{-/-}$ (AAV-Control) and *Hilnc*$^{-/-}$ (O/E-*Hilnc*) mice revealed the presence of numerous fat droplets in the WT and *Hilnc*$^{-/-}$ (O/E-*Hilnc*) mouse livers (Figure 5C), suggesting that hepatic overexpression of *Hilnc* in *Hilnc*$^{-/-}$ mice could restore liver lipid accumulation. In addition, the primary hepatocytes isolated from *Hilnc*$^{-/-}$ (O/E-*Hilnc*) mice showed greater lipid accumulation after OA treatment than those isolated from *Hilnc*$^{-/-}$ (AAV-control) mice (Figures 5F and 5G). These data verify the functional significance of hepatic *Hilnc* in HFD-induced hepatic steatosis.

Loss of *Hilnc* influences the PPAR signaling pathway in the liver

To investigate the mechanisms by which *Hilnc* regulates hepatic steatosis, we performed gene expression profiling of livers from WT and *Hilnc*$^{BM/BM}$ mice fed a NCD or HFD. Unsupervised cluster analysis of all genes clearly separated the samples according to genotype, demonstrating that loss of *Hilnc* induces marked transcriptional reprogramming of the liver under dietary excess (on a HFD). This included 702 genes that were upregulated and 524 genes that were downregulated in *Hilnc*$^{BM/BM}$ mice (Figure 6A, Supplementary Table 2). In contrast, only a minor percentage of genes were differentially expressed in *Hilnc*$^{BM/BM}$ mice compared with WT mice on the NCD (Figures S6A and S6B).

KEGG pathway analysis of the upregulated transcripts in *Hilnc*$^{BM/BM}$ mice on a HFD identified enrichment of pathways participating in cytokine-cytokine receptor interaction, Jak-STAT signaling, complement and coagulation cascades, and protein digestion and absorption (Figures S6C and S6D), while the downregulated genes were enriched in multiple pathways related to lipid metabolism, including metabolic pathways, fatty acid degradation, metabolism of xenobiotics by cytochrome P450 and PPAR signaling (Figure 6B).

Gene set enrichment analyses of decreased transcripts in *Hilnc*$^{BM/BM}$ mice revealed significant enrichment of the PPAR signaling pathway (Figure 6B), which includes a number of mitochondrial and peroxisomal fatty acid oxidation genes (Figure 6C) and can regulate lipid metabolism and fat formation and maintain metabolic homeostasis in many organs. The downregulation of some PPAR pathway genes, such as *Pparγ*, *Fabp1*, *Plin2* and *Scd1*, was confirmed by qPCR and western blot analyses (Figures 6D and 6E). We also detected the expression of PPARγ in WT and *Hilnc*$^{BM/BM}$ mice fed a NCD, and no significant difference was observed (Figure S6E). Interestingly, overexpression of *Hilnc* restored the expression of PPAR pathway genes in *Hilnc*$^{-/-}$ mice (Figure 6F). These results suggest that *Hilnc* is involved in the regulation of the PPAR signaling pathway under HFD conditions.

PPARs are lipid sensors that transcriptionally modulate metabolic processes in response to nutritional inputs (Venteclef et al., 2011). In our results, a significant difference was observed in the expression level of *Pparγ* in the liver of mice on a HFD (Figures 6D and 6E). Generally, the expression of *Pparγ* is low in human and mouse livers, being ~10–30% that in adipose tissue (Semple et al., 2006). However, hepatic *Pparγ* was recently described as a gene involved in hepatic steatosis and metabolic syndrome. It was reported that liver PPARγ2 was significantly upregulated in a rodent model of obesity (Vidal-Puig et al., 1996). *Ob/Ob* mice with liver-specific disruption of *Pparγ* exhibited a dramatic improvement in fatty liver but had exacerbated hyperglycemia and insulin resistance (Matsusue et al., 2003). The C3H mouse strain which does not express *Pparγ* in the liver is resistant to diet-induced hepatic steatosis, compared with C57BL/6 (B6) mice (Lee et al., 2012). To verify the function of *Pparγ* in fatty liver *in vivo*, we injected adenoviral sh-*Pparγ* into WT mice via tail veins to knockdown *Pparγ* in mouse livers (Figure 6G). Knockdown efficiency was verified by qPCR (Figure 6H). Hepatic *Pparγ* knockdown strongly improved hepatic steatosis (Figures 6I and 6J). These results are consistent with a previous study (Lee et al., 2012) and suggest that the PPAR signaling pathway is involved in diet-induced liver steatosis, and downregulation of the *Pparγ* gene in hepatocytes may prevent lipid accumulation.

Next, we tested whether *Hilnc* influences the PPAR signaling pathway *in vitro*. Knockdown of *Hilnc* in AML12 mouse hepatocytes with OA treatment by RNAi decreased the mRNA levels of *Pparγ* and *Fabp1* (Figures 6K). These data imply a strong relationship between *Hilnc* and *Pparγ* and that *Hilnc* regulates the PPAR pathway and the mRNA level of *Pparγ*.

Hilnc directly binds to IGF2BP2 and functions on *Pparγ* through IGF2BP2

LncRNAs can act in *cis* or in *trans* to modulate gene expression. Knocking out *Hilnc* (*Hilnc*$^{-/-}$) or mutating the Gli binding site in the *Hilnc* promoter region (*Hilnc*$^{BM/BM}$) failed to affect the mRNA expression level and protein level of the nearest-neighbor genes, *Fyn* and *Traf3ip2,* in the liver, which could indicate the lack of a *cis* regulatory function (Figure S7). Given that lncRNAs could function as protein recruiters to regulate protein stability and function, we then performed RNA pulldown in whole cell lysates of AML12 cells using biotin-labeled full-length *Hilnc* (*Hilnc*) to identify *Hilnc*-interacting proteins. A *Hilnc* antisense transcript (Ctr-1) and a 760-bp intron transcript (Ctr-2) were set as negative controls. The *Hilnc*-associated proteins were then separated by gel electrophoresis

and identified by mass spectrometry (MS) (Figure 7A). Insulin-like growth factor 2 mRNA binding protein 2 (IGF2BP2), a cytoplasmic mRNA-binding protein (mRBP) that regulates the life cycle of many client mRNAs by affecting RNA stability, localization and translation, was identified as a *Hilnc*-binding protein. The binding between *Hilnc* and IGF2BP2 was further confirmed by RNA pulldown followed by western blot analysis (Figure 7B). RNA immunoprecipitation (RIP) assays using an IGF2BP2-specific antibody showed that *Hilnc* was highly enriched in the IGF2BP2 antibody-retrieved complexes compared with the immunoglobulin G (IgG)-retrieved sample (Figure 7C). To further investigate the specific binding region on *Hilnc* that contributed to the interaction between *Hilnc* and IGF2BP2, *Hilnc* was divided into different segments according to the predicted spatial structure (1–300 bp, 300–535 bp, 535–650 bp, 650–779 bp). RNA pulldown using biotin-labeled *Hilnc* segments showed that 535–650 bp of *Hilnc* is responsible for its binding to IGF2BP2 (Figure 7D).

We next wanted to determine whether IGF2BP2 is functionally involved in diet-induced liver steatosis and in *Hilnc*-mediated regulation of the PPAR pathway. Liver-specific knockdown of IGF2BP2 improved diet-induced liver steatosis (Figures 7E–7G), which was consistent with the findings in hepatic *Hilnc*- or *Pparγ*-knockdown mice (Figures 4G and 6J). Knockdown of IGF2BP2 also reduced the mRNA and protein levels of *Pparγ* and *Fabp1* but did not affect the expression level of *Hilnc* (Figures 7H and 7I), implying that IGF2BP2 does not modulate the stability of *Hilnc* but might influence the stability of genes related to the PPAR pathway. Oil Red O staining and intracellular TG analysis showed that primary hepatocytes isolated from hepatic *Igf2bp2*-knockdown mice had decreased lipid accumulation after OA treatment (Figures 7J and 7K). Importantly, in primary hepatocytes with IGF2BP2 knockdown, further knockdown or overexpression of *Hilnc* had no effect on lipid accumulation, while overexpression of *Pparγ* increased lipid accumulation (Figures 7J and 7L), suggesting that *Hilnc* interacts with IGF2BP2 to regulate the PPAR pathway and subsequent lipid accumulation in hepatocytes. Photoactivatable ribonucleoside-enhanced CLIP (PAR-CLIP) sequencing in human embryonic kidney-293 cells showed that IGF2BP2 binds thousands of mRNAs, suggesting a wide range of gene targets (Hafner et al., 2010). It was reported recently that, in mouse liver, *Pparγ* is also an IGF2BP2 mRNA client (Regue et al., 2019). Thus, it is possible that *Hilnc* may be required for IGF2BP2-mediated posttranscriptional regulation of its targets (for example, PPARγ). To test this possibility, anti-IGF2BP2 immunoprecipitation assays were performed in liver samples from WT, *Hilnc*$^{-/-}$ or *Hilnc*-overexpressing mice (Hilnc$^{-/-}$ (O/E-Hilnc)). The results showed that *Pparγ* mRNA, *Igf2* mRNA and *Ddx3x* mRNA (employed as positive controls) were enriched in IGF2BP2 immunoprecipitation samples, while *Fabp1* mRNA and *Fasn* mRNA (employed as negative controls) were not enriched in these samples (Figure 7M). We also found that a lack of *Hilnc* decreased IGF2BP2 binding to *Pparγ* mRNA and *Igf2* mRNA, while overexpression of *Hilnc* in *Hilnc*$^{-/-}$ mouse livers restored IGF2BP2-*Pparγ* and IGF2BP2-*Igf2* binding (Figure 7M). And the presence or absence of *Hilnc* didn't influence IGF2BP2 binding to the mRNA of *Ddx3x*. Thus, our data suggested that *Hilnc* binds to IGF2BP2 and modulates IGF2BP2-mediated posttranscriptional regulation of a specific subset of metabolically active target genes (for example, *Pparγ*) in the liver.

Identification of the potential functional human homolog of *Hilnc*

Compared to protein-coding sequences, most of which are highly conserved throughout vertebrates, lncRNA sequences evolve very rapidly (Ulitsky and Bartel, 2013). The conservation of lncRNA between human and mouse is only 20%, and reduced to only 5% between human and fish (Hezroni et al., 2015). To identify human homology of *Hilnc,* we carried out detailed analyses on the potential transcripts from the *Hilnc* syntenic region in human genome (chr6: 111605457–111670597) and failed to identify any transcript (Figure S8A and S8B). We also blasted the sequence of *Hilnc* in NONCODE (www.noncode.org) and couldn't identify a similar transcript. Then we intent to perform a broader genome screening and to identify the potential functional homolog(s) of *Hilnc*.

We selected a human liver cell line (LO2), which showed lipid accumulation after OA treatment, to do screening. Based on our findings that *Hilnc* plays an important role in lipid metabolism, we performed RNA-seq in LO2 cells with and without OA treatment to identify the upregulated lncRNAs in response to intracellular lipid accumulation. We found that treating LO2 cells with OA could induce a large number of genes related to lipid metabolism process (Figure 8A), including *PPARγ* and *PLIN2*. We identified 158 lncRNAs that were upregulated (Fold change> 1.5) and 180 lncRNAs that were downregulated in LO2 cells treated with OA (Figure 8B, Supplementary Table 3). Among the top 100 upregulated lncRNAs, we found 20 lncRNAs that had at least one predicted Gli binding site near their TSS (±3 kb) with a high score in JASPAR (Fornes et al., 2020) (Figure 8C, Supplementary Table 4). Then we confirmed the upregulation of 14 lncRNAs in these 20 lncRNAs by qPCR (Figure 8D). Next, we generated siRNAs targeting those 14 lncRNAs and test whether knocking down those lncRNAs could influence lipid accumulation. Among those 14 lncRNAs, knocking down two novel lncRNAs, *ENST00000450804.3* and *ENST00000417084.1*, decreased lipid accumulation in LO2 cells treated with OA (Figure 8E). Interesting, knocking down *ENST00000417084.1* decreased the mRNA level of *PPARγ*, while knocking down *ENST00000450804.3* had no influence to the mRNA level of *PPARγ* (Figure 8F), implying that *ENST00000450804.3* and *ENST00000417084.1* influenced lipid accumulation by different mechanisms and *ENST00000417084.1* acted more like *Hilnc*. Thus, we focused our attention on *ENST00000417084.1* and named it human **H**edgehog signaling-**i**nduced **l**ong **n**on**c**oding RNA (*h-Hilnc*). We then performed RACE experiments and found that *h-Hilnc* is a 917-nucleotide transcript comprising four exons (Figure S8C). The *h-Hilnc* located in chr1: 207249067–207309121 (Figure S8D) in the human genome and lacked coding potential (Experimental Procedures) and had no predicted mouse homolog. The whole sequence of *h-Hilnc* was shown in Figure S8E. Similar to *Hilnc*, RIP assays showed that *h-Hilnc* could bind to IGF2BP2 (Figure 8G) and knocking down *h-Hilnc* also decreased IGF2BP2 binding to the mRNA of *PPARγ*, while knocking down *ENST00000450804.3* did not affect the binding of IGF2BP2 to *PPARγ* (Figure 8H). Interestingly, we noticed that OA treatment also upregulated the expression of *GLI1* in LO2 cells (Figure 8D), which is consistent with our results in mice liver (Figure 2B). It implied that *GLI1* could induce the expression of *h-Hilnc*. To test this possibility, we treated LO2 cells with OA and GANT61 together. We found that GANT61 significantly inhibited the upregulation of *h-Hilnc* in OA-treated LO2 cells (Figure 8I), implying that *h-Hilnc* could be directly induced by Hh signaling and GLI1. The *h-Hilnc* had a predicted

but non-consensus Gli binding site in its promoter region (Figure 8J). We then detected whether Hh signaling could regulate *h-Hilnc* through the Gli binding site in its promoter. The luciferase reporter assays showed that overexpression of GLI1 resulted in a significant increase in luciferase activity in the reporter construct carrying the WT Gli binding sites but failed to induce luciferase activity when the Gli binding site was mutated (Figure 8J). ChIP analysis also showed the binding of GLI1 to the *h-Hilnc* promoter (Figure 8K). These data suggested that *h-Hilnc* was regulated by Hh signaling and GLI1 and could influence lipid accumulation through regulating IGF2BP2-*PPARγ* binding, which makes it a potential functional human homolog of *Hilnc*.

DISCUSSION

In this study, we first characterized the biological roles of *Hilnc*, an Hh signaling-induced lncRNA, in diet-induced obesity and fatty liver. We demonstrated that the Hh signaling pathway transcriptionally regulates the expression of *Hilnc* by Gli *in vitro* and *in vivo*. Mutations of the Gli binding site in the *Hilnc* promoter dramatically decreased both constant and inducible *Hilnc* expression. An *in vivo* study demonstrated that mice with *Hilnc* depletion, induced by either deleting *Hilnc* or mutating the Gli binding site in the *Hilnc* promoter region, exhibited resistance to diet-induced obesity and fatty liver. We also identified a potential functional homolog of *Hilnc* and verified its role in lipid accumulation in human liver cells.

The detailed mechanisms by which lncRNAs coordinate with signaling pathways in biological processes remain largely unexplored. Only a few lncRNAs have been reported to be related to the Hh signaling pathway. Our current study together with other recent studies showed that Hh signaling may function through lncRNAs. For example, aberrant Hh signaling leads to overexpression of both Yap1 and H19, which is responsible for the pathogenesis and malignant transformation of osteoblastic osteosarcoma (Chan et al., 2014). Hh signaling maintains X-chromosome inactivation (XCI) in pluripotent cells by GLI-mediated expression of Tsix, the antisense repressor of XCI (Del Rosario et al., 2017). Our study also showed that Hh signaling regulates the expression of *Hilnc* by directly targeting the Gli-binding site in the *Hilnc* promoter region. Thus, the diverse transcription factor binding sites in the regulatory regions of lncRNAs may play an important role in connecting lncRNA expression with signaling activity.

LncRNAs function by interacting with distinct partners, such as transcription factors, ubiquitin ligases, mRBPs, and microRNAs (Yao et al., 2019b). The interaction between *Hilnc* and IGF2BP2 consequently impacts PPAR signaling to regulate lipid metabolism in liver, indicating the potential connections between lncRNAs and metabolic network. Global elimination of IGF2BP2 confers strong protection against obesity and fatty liver in mice fed a HFD through enhanced translation of Ucp1 mRNA and other mRNAs encoding mitochondrial proteins (Dai et al., 2015). Liver-specific IMP2 (named IGF2BP2 in humans) overexpression results in steatosis (Tybl et al., 2011), while liver-specific deletion of IMP2 reduces hepatic fatty acid oxidation and increases hepatic TG accumulation (Regue et al., 2019). Since we demonstrated that *Hilnc* could interact with IGF2BP2 and was important for IGF2BP2-mediated PPAR signaling regulation, our observation that $Hilnc^{BM/BM}$ and

Hilnc$^{-/-}$ mice are resistant to diet-induced obesity and fatty liver may provide new insight into the mechanism underlying IGF2BP2 functions. Since IGF2BPs are involved in regulating cell proliferation and organ development in many tissues (Christiansen et al., 2009; Li et al., 2012), and *Hilnc* is also highly expressed in other metabolic organs, it will be of great interest to identify the function of the *Hilnc*-IGF2BP2 regulation axis in other tissues.

The Hh signaling pathway has recently been identified as an important regulator of liver metabolism in NAFLD, and also in healthy, mature hepatocytes (Gao et al., 2018; Schmidt-Heck et al., 2015). Under normal chow diet, the hepatocyte-specific impairment of canonical Hh signaling by the conditional ablation of Smo results in considerable changes in liver lipid metabolism that ultimately leads to hepatic steatosis and down-regulation of Gli3 is sufficient for the development of steatosis (Matz-Soja et al., 2016). Hh signaling and its rhythmicity are deranged when steatosis is caused by nutritional challenges, such as HFD treatment (Marbach-Breitruck et al., 2019). Humans with holoprosencephaly (a disease caused by SHH signaling mutations) have a higher incidence of fatty liver and Gli2$^{+/-}$ mice develop more fatty liver when exposed to fatty liver-inducing diets (Guillen-Sacoto et al., 2017). Interesting, it is also reported that pharmacologic Smo inhibitors, LED225, reduce HFD-induced hepatic steatosis, but liver specific deletion of Smo reduced macrophage activation and inhibited pro-inflammatory cytokine expression, while it did not significantly alter fat accumulation in NAFLD (Kwon et al., 2016). In our cases, we found that *Hilnc* was regulated by Hh signaling and directly by Gli1 in NAFLD and loss of *Hilnc* reduced HFD-induced hepatic steatosis, suggesting that Hh signaling could promote the development of diet-induced hepatic steatosis and NAFLD through Gli1 and *Hilnc*. The diverse findings about the role of Hh signaling in lipid metabolism implied that there might have complicated mechanisms in the regulation of Hh signaling to lipid metabolism and Gli1, Gli2 or Gli3 might have different role in hepatic steatosis under either physiological or pathological conditions. The identified Hh-Gli1-*Hilnc*-IGF2BP2 axis could be a new mechanism and a supplement by which Hh signaling participates in lipid metabolism and the development of NAFLD through Gli1.

A major challenge in lncRNA studies is that it is often more difficult to infer the function of a lncRNA based on its evolutionary history because the current comparative genomic tools cannot easily detect homology between lncRNAs (Ulitsky and Bartel, 2013). We couldn't find a human homolog of *Hilnc* from its syntenic region in the human genome and from sequence similarity. However, we identified a potential functional human homolog of *Hilnc*, *h-Hilnc* (*ENST00000417084.1*). Similar to *Hilnc*, *h-Hilnc* could influence lipid accumulation through IGF2BP2 and was regulated by Hh signaling and Gli1 in LO2 cells. We noticed that the Gli binding site in *h-Hilnc* promoter is non-consensus site, implying that the regulation of Hh signaling to *h-Hilnc* might not as strong as that to *Hilnc* in mouse and Hh signaling might also regulate other potential human lncRNAs. The existence of the functional human homolog of *Hilnc* proved the conserved role of Hh signaling and Gli1 in mammals and suggested the importance of other uncharacterized lncRNAs that are not conserved.

In summary, our work identified an Hh signaling-related lncRNA, *Hilnc*, and revealed a novel mechanism by which Hh signaling regulates lipid metabolism via the *Hilnc*-IGF2BP2 axis. The newly identified Hh-*Hilnc*-IGF2BP2 axis provides an additional understanding of how signaling pathways regulate lncRNAs and how lncRNAs participate in systemic metabolism. It would be interesting to examine the activity of this pathway in other organs and diseases.

MATERIALS and METHODS

RNA sequencing and Bioinformatic Analyses

For lncRNA sequencing, a total amount of 3 μg RNA per sample was used as input material for the RNA sample preparations. Firstly, ribosomal RNA was removed by Epicentre Ribo-zero™ rRNA Removal Kit (Epicentre, USA), and rRNA free residue was cleaned up by ethanol precipitation. Subsequently, sequencing libraries were generated using the rRNAdepleted RNA by NEBNext® Ultra™ Directional RNA Library Prep Kit for Illumina® (NEB, USA) following manufacturer's recommendations. The clustering of the index-coded samples was performed on a cBot Cluster Generation System using TruSeq PE Cluster Kit v3-cBot-HS (Illumia) according to the manufacturer's instructions. After cluster generation, the libraries were sequenced on an Illumina Hiseq 4000 platform and 150 bp paired-end reads were generated. Raw data (raw reads) of fastq format were firstly processed through in-house perl scripts. In this step, clean data (clean reads) were obtained by removing reads containing adapter, reads on containing ploy-N and low quality reads from raw data. At the same time, Q20, Q30 and GC content of the clean data were calculated. All the downstream analyses were based on the clean data with high quality. Cuffdiff (v2.1.1) was used to calculate FPKMs of both lncRNAs and coding genes in each sample. FPKM, expected number of Fragments Per Kilobase of transcript sequence per Millions base pairs sequenced, considers the effect of sequencing depth and gene length for the reads count at the same time, and is currently the most commonly used method for estimating gene expression levels.

For transcriptome sequencing, a total amount of 1 μg RNA per sample was used as input material for the RNA sample preparations. Sequencing libraries were generated using NEBNext® UltraTM RNA Library Prep Kit for Illumina® (NEB, USA) following manufacturer's recommendations and index codes were added to attribute sequences to each sample. The clustering of the index-coded samples was performed on a cBot Cluster Generation System using TruSeq PE Cluster Kit v3-cBot-HS (Illumia) according to the manufacturer's instructions. After cluster generation, the library preparations were sequenced on an Illumina Novaseq platform and 150 bp paired-end reads were generated. featureCounts v1.5.0-p3 was used to count the reads numbers mapped to each gene. And then FPKM of each gene was calculated based on the length of the gene and reads count mapped to this gene.

Prior to differential gene expression analysis, for each sequenced library, the read counts were adjusted by edgeR program package through one scaling normalized factor. Differential expression analysis of two conditions was performed using the edgeR R package (3.18.1). The P values were adjusted using the Benjamini & Hochberg method.

Corrected P-value of 0.05 and absolute fold change of 1.5 were set as the threshold for significantly differential expression.

Gene Ontology (GO) enrichment analysis of differentially expressed genes was implemented by the cluster Profiler R package, in which gene length bias was corrected. GO terms with corrected P value less than 0.05 were considered significantly enriched by differential expressed genes.

KEGG is a database resource for understanding high-level functions and utilities of the biological system, such as the cell, the organism and the ecosystem, from molecular-level information, especially large-scale molecular datasets generated by genome sequencing and other high-through put experimental technologies (http://www.genome.jp/kegg/). We used cluster Profiler R package to test the statistical enrichment of differential expression genes in KEGG pathways.

The protein-coding potential of *Hilnc* sequence was evaluated by two widely used algorithms, Coding Potential Calculator (CPC)(Kong et al., 2007), and Coding Potential Assessment Tool (CPAT)(Wang et al., 2013). For CPC, transcripts with scores more than 1 are classified as “coding,” less than −1 as “non coding,” and between −1 and 1 are marked as “weak non coding” ([−1, 0]) or “weak coding” ([0, 1]), respectively. The CPC score of two *Hilnc* transcripts and *h-Hilnc* are −1.13484, −1.07993 and 0.03473, which was calculated with http://cpc.cbi.pku.edu.cn/programs/run_cpc.jsp using default thresholds. For CPAT, mouse coding probability (CP) cutoff is 0.44, so transcripts with scores more than 0.44 are classified as “coding” and less than 0.44 as “non-coding.” The coding potential of two *Hilnc* transcripts and *h-Hilnc* calculated with CPAT using default thresholds are 0.0105, −0.0111 and 0.0101, also indicating that they are noncoding transcript.

Genomic Analysis of *Hilnc* and *h-Hilnc*

5’ and 3’ RACE was performed using FirstChoice RLM-RACE kit (Ambion) on NIH-3T3 cell RNA and LO2 cell RNA, and products were cloned using TOPO TA cloning kit (Invitrogen). See Supplementary Table 5 for primer sequences.

Plasmid construction, generation of stable cell lines and ESCs

Hilnc and Flag tagged Gli1, Gli2 and Pparγ were cloned to vector pcDNA3.1. pGL3-*Hilnc*-promoter and pGL2-*h-Hilnc*-promoter was cloned by inserting the *Hilnc* promoter (~1,000 bp upstream of *Hilnc* TSS) and *h-Hilnc* promoter into pGL3-Basic Vector (Promeg). Deletion and random mutation of the Gli binding site of the promoter region were created with the KOD-Plus Mutagenesis Kit (TOYOBO). See Supplementary Table 5 for primer sequences.

To generate *Hilnc* promoter mutated NIH-3T3 cell lines and haploid mouse ESCs, sgRNA(sgRNA-1) targeting the Gli binding site in *Hilnc* promoter region was designed and inserted into CRISPR/Cas9 vector px330-mCherry. The homologous arm sequences (chr11:39,613,549–39,614,780) for donor plasmids were amplified from the genomic DNA of NIH-3T3 cells. Then the Gli binding site (GACCACCCA) in the homologous arm was

randomly mutated to GTATGCATG, which didn't generate any known transcription factor binding sites.

To generate *Hilnc* KO haploid mouse ESCs, three sgRNAs (sgRNA-2–1, sgRNA2–2, sgRNA-3) (two targeting upstream and one targeting downstream of the *Hilnc* exons 2 and 3) were designed and inserted into CRISPR/Cas9 vector px330-mCherry.

sgRNA-1: CCATTATGGTAGTACCCTTCTGG;

sgRNA-2–1: GCTTCGTAAGTGATAGACACTGG;

sgRNA-2–2: AGGTTTATTGCTCAGGCGTGTGG;

sgRNA-3: TTCCACTCTCTGGTACCCGCAGG.

Generation of *Hilnc* knockout (*Hilnc*$^{-/-}$) mice and *Hilnc* promoter region mutated (*Hilnc*$^{BM/BM}$) mice

Protocol of generating genetically modified mice was described in ref(Yang et al., 2014). Briefly, genetically modified haploid ESCs were injected into metaphase II oocytes and SrCl2 stimulus activation, full-term pups (referred to as semi-cloned mice) were generated after transferring the embryos to the uterus of pseudo-pregnant mice. F1 offspring carrying the mutant allele were identified by PCR using the strategy indicated in Supplemental Figure 3. The PCR primer sequences for *Hilnc*$^{-/-}$ mice were as follows: primer 1 (P1), 5'-TTGCAAATATTCCCTGGAGGGT-3'; primer 2 (P2), 5'-ATTCACAGCTAGCCATTGTTGG-3'; primer 3 (P3), 5'-CTTAAAGTCCACTGAGTCGCTG-3'. The PCR products expected were 880 bp for the WT allele (P1 and P2), and 770 bp for the recombined allele (P1 and P3). The PCR primer sequences for *Hilnc*$^{BM/BM}$ mice were as follows: primer 4 (P4), 5'- GAGAAGAAACACTGGATCTTGG-3'; primer 5 (P5), 5'- CAAGTTTTAGAGACCACCCATTATGG-3'; primer 6 (P6), 5'-CAAGTTTTAGAGTATGCATGTTATGG-3'. The PCR products expected were 375 bp for the WT allele (P4 and P5), and 375 bp for the recombined allele (P4 and P6).

During experiments, the mice were often processed during 12:00 ~ 15:00 PM.

In Vivo effect of Adenovirus

Six-week-old male WT mice were injected with sh-*Hilnc*, sh-*Igf2bp2*, sh-*Pparγ* or sh-Control recombinant adenovirus. Six-week-old male *Hilnc*$^{-/-}$ mice were injected with AAV8-*Hilnc* (O/E-*Hilnc*), or AAV8-GFP (AAV-Control) recombinant adenovirus. Recombinant adenovirus (2×10^9 pfu) was delivered by tail-vein injection to mice. All adenoviruses were made by Hanbio (Shanghai, China).

sh-*Hilnc*: 5′- CCUAAACUGGCGCCACAUUTT -3′;

sh-*Igf2bp2*: 5′- GGGUAAAGUGGAAUUGCAUTT -3′;

sh-*Pparγ*: 5′- GAAGUUCAAUGCACUGGAATT -3′

Indirect calorimetry, food intake and activity

For analysis of body weight and food intake, mice were kept at normal ambient temperature of 23 ± 1°C and had free access to water and food. Measurements of energy expenditure were performed using a customized indirect calorimetric system (Columbus×Oxymax/CLAMS). After weaning, age- and sex-matched control and *Hilnc*$^{BM/BM}$ mice were housed individually and acclimated to metabolic cages and for 3 days prior to data collection. Total oxygen consumption (VO_2) and carbon dioxide production (VCO_2) were measured continuously by indirect calorimetry. The value of respiratory exchange ratio and energy expenditure for each individual cage was recorded every 30 min and converted by CLAMS software. Ambulatory activity was determined simultaneously with the collection of calorimetry data using CLAMS. Food intake was recorded continuously over a 24 hours period during which chow was available ad libitum. Consecutive adjacent infrared beam breaks in either the x- or z-axes were scored as an activity count, and a tally was recorded every 10 min.

Cell culture

NIH-3T3 cells were cultured in DMEM (Invitrogen, Carlsbad, CA) with 10% NCS and antibiotics at 37 °C with 5% CO_2 in a humidified incubator (Thermo, Waltham, MA). HEK293T cells were cultured in DMEM supplemented with 10% FBS. AML12 cells were maintained in DMEM/F12 medium (Sigma) containing 10% FBS, 1% ITS Liquid Media Supplement (Sigma), 40 ng/ml Dexamethasone. LO2 cells were maintained in RPMI 1640 medium (Sigma) containing 10% FBS. Cells were obtained from Shanghai Life Academy of Sciences cell library (Shanghai, China), then the short tandem repeat analysis was performed to authenticate the cell lines. Multiple aliquots were frozen within 10 days when the cells were purchased and thawed.

Mouse primary hepatocytes were isolated from livers of male C57BL/6J mice, *Hilnc*$^{BM/BM}$ mice, *Hilnc*$^{-/-}$ (AAV-Control) mice, *Hilnc*$^{-/-}$ (O/E-*Hilnc*) mice and *Igf2bp2* knockdown mice (8 weeks old) as previously reported(Li et al., 2010). Briefly, liver cells were isolated by injection of 0.5 mg/mL type collagenase (Sigma) through the inferior vena cava after anaesthesia in mice. Trypan blue dyes were used to detect cell activity (70% or more). Then, primary hepatocytes were cultured in Williams E medium (Sigma) containing 1% (v/v) penicillin/streptomycin (10,000 U/μg/ml; Sigma), 0.5% (v/v) gentamycin (10 mg/ml; Gibco), 0.04% (v/v) fungizone (amphotericin B, 250 μg/ml; Gibco), 1% (v/v) 200 mM L-glutamine (Sigma) and 1% (v/v) nonessential amino acids (Gibco). Primary hepatocytes isolated from *Igf2bp2* knockdown mice were transfected with empty plasmid, siRNA-*Hilnc*, pcDNA3.1-*Hilnc* and pcDNA3.1-Flag-Pparγ for 24 hours, and the medium was replaced with 0.5 mM oleic acid (OA) containing fresh medium for another 24 hours. Cells were then collected for further analysis.

Separation of nuclei and cytoplasm

Nucleo-cytoplasmic separation was performed using the PARIS™ Kit (ambion) according to the manufacturer's instruction. Briefly, whole cells were washed with ice-cold PBS, then resuspended in ice-cold cell fractionation buffer. Cytoplasmic fraction and the nuclear pellet

were separated by centrifugation. Protein and RNA were isolated from each fraction and analyzed by western blot and qPCR.

Immunoblot

Cells were lysed in Cell Lysis Buffer (Cell Signaling Technology) supplemented with Complete protease inhibitor cocktail (Roche) and followed by sonication and centrifugation to get the clear cell lysate. Tissues were extracted in ice-cold lysis buffer (10 mM Tris-HCl (pH 8.0), 140 mM KCl, 1 mM $MgCl_2$, 0.1 M NaF, 0.1% NP-40) with Complete protease inhibitor cocktail using tissue lyser (Qiagene). Tissue or cell lysates were resolved on a 4–12% SDS polyacrylamide gels (Invitrogen) and electro transferred to a PVDF membrane. Protein was detected by chemiluminescence (ECL kit, Thermo Scientific). The pictures were captured by Mini Chemiluminescent / Fluorescent Imaging and Analysis System (SNSITECH). The antibodies used were listed in Supplementary Table 6.

RNA fluorescence in situ hybridization (FISH) and Immunocytochemistry

Digoxigein (DIG)-labeled sense (F, forward) or anti-sense (R, reverse) *Hilnc* probe were synthesized using DIG RNA labeling kit (Roche). For RNA FISH, the cells were seeded onto a multichamber culture slide (BD Falcon), fixed and permeabilized as described in ref (Kawaguchi et al., 2015). Then the slides were hybridized with DIG-labeled RNA probe followed by excess RNA probes digestion and four times washes. The detection procedure was performed using the HNPP Fluorescent Detection Set (Roche) as the manufacturer's protocol.

RNA immunoprecipitation

AML12 cells and LO2 cells were harvested and lysed with Cell Lysis Buffer (Cell Signaling Technology) supplemented with 1 U/μl RNase Inhibitor and Complete protease inhibitor cocktail (Roche). Mouse livers were harvested after sacrifice and extracted using tissue lyser (Qiagene) in ice cold Cell Lysis Buffer (Cell Signaling Technology) supplemented with 1 U/μl RNase Inhibitor and Complete protease inhibitor cocktail (Roche) and extracted for 10 min. The lysate was centrifuged for 10 min at 14,000 rpm, and supernatant was transferred to a fresh 1.5 mL tube. Total protein was measured by Bradford assay and 2mg of cytoplasmic lysate protein was subjected to immunoprecititation.

IGF2BP2 antibody (Proteintech) and normal rabbit IgG were added to the clarified lysate and hybridized for 4 hours (or overnight) at 4°C. Then 50μl Protein A Magnetic Beads (NEB) were added to the samples and hybridized for 2 hours at 4°C. After five washes using NT2 (+) buffer (50 mM Tris-HCl pH7.0, 150 mM NaCl, 1 mM $MgCl_2$, 0.05% NP-40, 1 mM PMSF, 10 mM Ribonucleoside Vanadyl Complex (Sigma), the RNA and protein on beads were isolated using TRIzol according to the manufacturer's instructions. RNA fraction was subjected to qPCR analysis.

RNA pulldown assay

For transcription *in vitro*, biotin-labeled sense or anti-sense RNAs were synthesized using DIG RNA labeling kit (Roche) and Biotin RNA Labeling Mix (Roche). And the isolated 3 μg biotin-labeled RNA was heated to 90°C for 2 min to disrupt the secondary structure, and

placed on ice for 2 min to form the proper secondary structure. The 2×10^7 cells were lysed in Cell Lysis Buffer (Cell Signaling Technology) supplemented with Complete protease inhibitor cocktail and 1 U/μl RNase Inhibitor followed by sonication and centrifugation to get the clear cell lysate. Then the lysate was precleared with 50μl streptavidin-coupled beads (Pierce Streptavidin Magnetic Beads, Thermo fisher) by rotating at 4°C for 30 min. Then folded RNA were added to the precleared cell lysate and rotated at room temperature for 1 hour. 100 μl washed streptavidin-coupled beads were added to the reaction and at 4°C for 4 hours followed by four washes using the NT2 (+) buffer supplemented with 1 mM PMSF, 10 mM Ribonucleoside Vanadyl Complex. The protein on beads were separated by SDS-PAGE followed by silver staining and mass spectrometry (MS) identification.

Quantitative real time PCR

Total RNA of cells or tissues were lysed in TRIzol (Invitrogen) for total RNA isolation following standard protocol. For qPCR, 0.5 μg RNA was used for reverse transcription with ReverTra Ace qPCR RT Master Mix with gDNA Remover (TOYOBO, FSQ-301). qPCR was performed with SYBR® Green Realtime PCR Master Mix (TOYOBO, QPK-201). The $2^{-\Delta\Delta Ct}$ method was used for quantification. The primer pairs used were listed in Supplementary Table 5.

Luciferase assay

For Dual-Luciferase reporter assays, PcDNA3.1-Flag-Gli1/Gli2 plasmids were transfected in 293T cells together with the pGL3-*Hilnc*/pGL3-*h-Hilnc* reporter and Renilla luciferase, which was used to normalize the transfection efficiency. After 48 hours, cell lysates were harvested, and Dual-Luciferase activities were measured according to the manufacturer's instructions (Promega).

Knockdown

10nM siRNA were transfected into the indicated cells using the RNA iMAX regent (Thermo fisher) as the standard procedures. The mouse *Hilnc* specific sequence (designed and synthesized by Genepharma) 5'- CCUAAACUGGCGCCACAUU -3' was for siRNA-1, 5'- GGUCAUACCCAUGAGGAAG -3' was for siRNA-2. And the no-target sequence 5'-UUCUCCGAACGUGUCACGU-3' was for negative control. The human sequence 5'- CAGGCAUCCAACAAUAAUATT -3' and 5'- CAGGAAGUCAACAGAUAAUTT -3' were for siRNA-ENST00000417084.1; 5'- GAGCCUGUCUUGAGCAUAATT -3' and 5'- GGUGCAGCAUUCUGUUGAUTT -3' were for siRNA-ENST00000450804.3.

Chromatin immunoprecipitation (ChIP).

ChIP experiments were carried out in NIH-3T3 cells and LO2 cells according to a standard protocol. The cell lysate transfected with PcDNA3.1-Flag-Gli1/Gli2 or PcDNA3.1-Flag-GLI1 was sonicated for 40 min (30s on/30s off), and chromatin was divided into fragments ranging mainly from 100 to 300 bp in length. Immunoprecipitation was then performed by using antibodies against Flag tag, and normal IgG was used as a control. The immunoprecipitated DNA was collected with QIAQIUCK PCR Purification Kit

(250). Purified DNA was performed with ChIP-PCR. The primers used were shown in Supplementary Table 5.

Glucose and insulin tolerance tests

For glucose tolerance tests, high fat fed mice were fasted overnight. Twenty percent D-Glucose (Sigma) (1 g/kg body weight) was administered by intraperitoneal injection. At 0, 20, 40, 60, 120 min after administration, blood was collected by tail vein bleeding. Glucose levels were measured by Roche glucometer. For insulin tolerance tests, high fat fed mice were fasted for 5 hours. Human insulin (Yeasen) 0.4 U/kg was injected intraperitoneally. At 0, 20, 40, 60, and 90 min after injection, tail vein blood was drawn and glucose levels measured as above.

Histological, lipid staining and Immunofluorescence

Freshly dissected mouse livers and white adipose tissue (WAT) were removed and fixed with 4% paraformaldehyde and embedded in paraffin. Cryosections (4 μm) were obtained and tissue sections were stained with H&E following standard protocol.

For lipid staining, Cells were washed twice with PBS and fixed with 7.5% formaldehyde in PBS for 30 min. After two washes in PBS, cells were stained for 15 min in freshly diluted Oil Red O solution. The dishes were then rinsed in water and counterstained with hematoxylin for 10 sec. Freshly dissected mouse liver was fixed in 4% paraformaldehyde at 4°C for 1 hour. After fixation, tissues were washed in PBS for three times, dehydrated in 30% sucrose overnight at 4°C and embedded in OCT. Cryosections (10μm) were obtained and air-dried afterwards at room temperature. Then the sections of liver were stained with oil Red O for 10 min, washed, and counterstained with hematoxylin for 20 sec. Representative photomicrographs were captured at 100x or 200x magnification using a system incorporated in the microscope.

For immunofluorescence staining, dried sections were washed in PBS and then blocked with 1% BSA and 0.1% Triton X-100 in PBS for 30 min at room temperature. Sections were incubated overnight at 4°C with the Rabbit anti-ZsGreen (Clontech, 632474, 1:10000). ZsGreen antibody was detected using fluorescent conjugated secondary antibodies (Alexa Fluor 488; Invitrogen). Sections were stained with DAPI (4,6-diamidino-2-phenylindole) and mounted with Aqua-Ploy/mount (Polysciences). Immunostaining images were acquired by Olympus fluorescence microscope (BX53) and Leica TCS SP8 confocal microscope. ImageJ software was used to analyze the collected image.

De novo lipogenesis

DNL activity was determined by the incorporation of [^{14}C] acetate into the lipids.

For the liver slices, the liver was taken from mice that had been anesthetized with isoflurane (Escain; Merck Hoei). The incubation medium consisted of Dulbecco's modified Eagle's medium (Invitrogen) and 0.5 mM [1-^{14}C] sodium acetate (final concentrations, 29.6 MBq/mmol and 2.11 GBq/mmol; GE Healthcare Bio-Sciences Corp.) and was aerated with 5% CO_2–95% O_2 gas for at least 20 min prior to use. The liver slices (approximately 20

to 25 mg) were incubated with the incubation medium for 90 min at 37°C. After the incubation period, the liver slices were heated with ethanolic KOH for 1 hour at 70°C, and nonsaponified lipids were removed with petroleum ether.

The resulting aqueous sample solutions obtained either from the liver slices or the hepatocytes were acidified, and then the lipids were extracted with petroleum ether. Radioactivity in the lipid fraction was counted with a liquid scintillation counter (Tri-Carb 2500; Perkin-Elmer).

Triglyceride (TG) Assay in the liver and primary hepatocytes

Intracellular and liver triglycerides were assayed using a triglyceride assay kit (GPO-POD; Applygen Technologies Inc., Beijing, China) according to the manufacturer's recommended protocol.

Statistical Analysis

All data were presented as the mean ± SEM. The results were analyzed using one- or two-way analysis of variance, followed by a least significant difference tukey's test, and $p < 0.05$ was considered statistically significant. GraphPad Prism (v.8) and the Sangerbox tools (http://www.sangerbox.com/tool) were used for statistical calculations and generation of plots. The "n" in the study represented the number of biological replicates and was indicated in the manuscript.

Supplementary Material

Refer to Web version on PubMed Central for supplementary material.

ACKNOWLEDGEMENTS

We would like to thank animal facility for the animal husbandry, and technical supports from Core Facility for Cell Biology and Genome Tagging Project (GTP) Center, at CEMC. We acknowledge Dr. Weiwei Yang for the providing reagents and helpful comments. This study was supported by grants from the National Key Research and Development Program of China (No. 2020YFA0509000, 2017YFA0503600 and 2017YFA0505500), the National Natural Science Foundation of China (31630047, 81874201, 81830054 and 81772723), the Strategic Priority Research Program of the Chinese Academy of Sciences (XDB19020100 and XDA16020905), the Basic Frontier Science Research Program of Chinese Academy of Sciences (No. ZDBS-LY-SM015), the CAS-VPST Silk Road Science Fund 2019 (GJHZ201968) and Science and Technology Commission of Shanghai Municipality (20Y11908300).

Data availability

RNA-seq data can be viewed in NODE (http://www.biosino.org/node) by pasting the accession OEP001927 into the text search box or through the URL: http://www.biosino.org/node/project/detail/OEP001927. Source Data for each figure are provided. Other data that support the findings of this study are available from the corresponding author upon reasonable request.

Abbreviations:

Hh	Hedgehog

Hilnc	Hedgehog signaling induced long noncoding RNA
h-Hilnc	Human *Hilnc*
Gli1/2/3	glioma-associated oncogene homolog 1/2/3
SAG	Smo receptor agonist
SHH	sonic hedgehog signaling ligand
IGF2BP2	insulin-like growth factor 2 mRNA binding protein 2
NCD	normal chow diet
HFD	high fat diet.
MCD	methionine and choline deficient l-amino acid diet
TG	triglyceride

References

Chan LH, Wang W, Yeung W, Deng Y, Yuan P, and Mak KK (2014). Hedgehog signaling induces osteosarcoma development through Yap1 and H19 overexpression. Oncogene 33, 4857–4866. [PubMed: 24141783]

Chen LL (2016). Linking Long Noncoding RNA Localization and Function. Trends Biochem Sci 41, 761–772. [PubMed: 27499234]

Choi SS, Omenetti A, Syn WK, and Diehl AM (2011). The role of Hedgehog signaling in fibrogenic liver repair. Int J Biochem Cell Biol 43, 238–244. [PubMed: 21056686]

Christiansen J, Kolte AM, Hansen T, and Nielsen FC (2009). IGF2 mRNA-binding protein 2: biological function and putative role in type 2 diabetes. J Mol Endocrinol 43, 187–195. [PubMed: 19429674]

Claussnitzer M, Dankel SN, Kim KH, Quon G, Meuleman W, Haugen C, Glunk V, Sousa IS, Beaudry JL, Puviindran V, et al. (2015). FTO Obesity Variant Circuitry and Adipocyte Browning in Humans. N Engl J Med 373, 895–907. [PubMed: 26287746]

Dai N, Zhao L, Wrighting D, Kramer D, Majithia A, Wang Y, Cracan V, Borges-Rivera D, Mootha VK, Nahrendorf M, et al. (2015). IGF2BP2/IMP2-Deficient mice resist obesity through enhanced translation of Ucp1 mRNA and Other mRNAs encoding mitochondrial proteins. Cell Metab 21, 609–621. [PubMed: 25863250]

Del Rosario BC, Del Rosario AM, Anselmo A, Wang PI, Sadreyev RI, and Lee JT (2017). Genetic Intersection of Tsix and Hedgehog Signaling during the Initiation of X-Chromosome Inactivation. Dev Cell 43, 359–371 e356. [PubMed: 29107559]

El-Agroudy NN, El-Naga RN, El-Razeq RA, and El-Demerdash E (2016). Forskolin, a hedgehog signalling inhibitor, attenuates carbon tetrachloride-induced liver fibrosis in rats. Br J Pharmacol 173, 3248–3260. [PubMed: 27590029]

Fornes O, Castro-Mondragon JA, Khan A, van der Lee R, Zhang X, Richmond PA, Modi BP, Correard S, Gheorghe M, Baranašić D, et al. (2020). JASPAR 2020: update of the open-access database of transcription factor binding profiles. Nucleic Acids Res 48, D87–d92. [PubMed: 31701148]

Gao L, Zhang Z, Zhang P, Yu M, and Yang T (2018). Role of canonical Hedgehog signaling pathway in liver. Int J Biol Sci 14, 1636–1644. [PubMed: 30416378]

Geisler S, and Coller J (2013). RNA in unexpected places: long non-coding RNA functions in diverse cellular contexts. Nat Rev Mol Cell Biol 14, 699–712. [PubMed: 24105322]

Guillen-Sacoto MJ, Martinez AF, Abe Y, Kruszka P, Weiss K, Everson JL, Bataller R, Kleiner DE, Ward JM, Sulik KK, et al. (2017). Human germline hedgehog pathway mutations predispose to fatty liver. J Hepatol 67, 809–817. [PubMed: 28645738]

Guy CD, Suzuki A, Zdanowicz M, Abdelmalek MF, Burchette J, Unalp A, Diehl AM, and Nash CRN (2012). Hedgehog pathway activation parallels histologic severity of injury and fibrosis in human nonalcoholic fatty liver disease. Hepatology 55, 1711–1721. [PubMed: 22213086]

Hafner M, Landthaler M, Burger L, Khorshid M, Hausser J, Berninger P, Rothballer A, Ascano M Jr., Jungkamp AC, Munschauer M, et al. (2010). Transcriptome-wide identification of RNA-binding protein and microRNA target sites by PAR-CLIP. Cell 141, 129–141. [PubMed: 20371350]

Hallikas O, Palin K, Sinjushina N, Rautiainen R, Partanen J, Ukkonen E, and Taipale J (2006). Genome-wide prediction of mammalian enhancers based on analysis of transcription-factor binding affinity. Cell 124, 47–59. [PubMed: 16413481]

Hezroni H, Koppstein D, Schwartz MG, Avrutin A, Bartel DP, and Ulitsky I (2015). Principles of long noncoding RNA evolution derived from direct comparison of transcriptomes in 17 species. Cell Rep 11, 1110–1122. [PubMed: 25959816]

Huarte M (2015). The emerging role of lncRNAs in cancer. Nat Med 21, 1253–1261. [PubMed: 26540387]

Ingham PW, and McMahon AP (2001). Hedgehog signaling in animal development: paradigms and principles. Genes Dev 15, 3059–3087. [PubMed: 11731473]

Kasper M, Jaks V, Fiaschi M, and Toftgard R (2009). Hedgehog signalling in breast cancer. Carcinogenesis 30, 903–911. [PubMed: 19237605]

Kawaguchi T, Tanigawa A, Naganuma T, Ohkawa Y, Souquere S, Pierron G, and Hirose T (2015). SWI/SNF chromatin-remodeling complexes function in noncoding RNA-dependent assembly of nuclear bodies. Proc Natl Acad Sci U S A 112, 4304–4309. [PubMed: 25831520]

Kinzler KW, and Vogelstein B (1990). The GLI gene encodes a nuclear protein which binds specific sequences in the human genome. 10, 634–642.

Kong L, Zhang Y, Ye ZQ, Liu XQ, Zhao SQ, Wei L, and Gao G (2007). CPC: assess the protein-coding potential of transcripts using sequence features and support vector machine. Nucleic Acids Res 35, W345–349. [PubMed: 17631615]

Kwon H, Song K, Han C, Chen W, Wang Y, Dash S, Lim K, and Wu T (2016). Inhibition of hedgehog signaling ameliorates hepatic inflammation in mice with nonalcoholic fatty liver disease. Hepatology 63, 1155–1169. [PubMed: 26473743]

Lauth M, Bergström Å, Shimokawa T, and Toftgård R (2007). Inhibition of GLI-mediated transcription and tumor cell growth by small-molecule antagonists. Proceedings of the National Academy of Sciences 104, 8455.

Lee EY, Ji H, Ouyang Z, Zhou B, Ma W, Vokes SA, McMahon AP, Wong WH, and Scott MP (2010). Hedgehog pathway-regulated gene networks in cerebellum development and tumorigenesis. Proc Natl Acad Sci U S A 107, 9736–9741. [PubMed: 20460306]

Lee JT (2012). Epigenetic regulation by long noncoding RNAs. Science 338, 1435–1439. [PubMed: 23239728]

Lee YJ, Ko EH, Kim JE, Kim E, Lee H, Choi H, Yu JH, Kim HJ, Seong JK, Kim KS, et al. (2012). Nuclear receptor PPARgamma-regulated monoacylglycerol O-acyltransferase 1 (MGAT1) expression is responsible for the lipid accumulation in diet-induced hepatic steatosis. Proc Natl Acad Sci U S A 109, 13656–13661. [PubMed: 22869740]

Li WC, Ralphs KL, and Tosh D (2010). Isolation and culture of adult mouse hepatocytes. Methods Mol Biol 633, 185–196. [PubMed: 20204628]

Li Z, Gilbert JA, Zhang Y, Zhang M, Qiu Q, Ramanujan K, Shavlakadze T, Eash JK, Scaramozza A, Goddeeris MM, et al. (2012). An HMGA2-IGF2BP2 axis regulates myoblast proliferation and myogenesis. Dev Cell 23, 1176–1188. [PubMed: 23177649]

Lin BJ, Zhu JY, Ye J, Lu SD, Liao MD, Meng XC, and Yin GQ (2020). LncRNA-XIST promotes dermal papilla induced hair follicle regeneration by targeting miR-424 to activate hedgehog signaling. Cell Signal 72, 109623. [PubMed: 32243962]

Marbach-Breitruck E, Matz-Soja M, Abraham U, Schmidt-Heck W, Sales S, Rennert C, Kern M, Aleithe S, Spormann L, Thiel C, et al. (2019). Tick-tock hedgehog-mutual crosstalk with liver circadian clock promotes liver steatosis. J Hepatol 70, 1192–1202. [PubMed: 30711403]

Matsusue K, Haluzik M, Lambert G, Yim SH, Gavrilova O, Ward JM, Brewer B Jr., Reitman ML, and Gonzalez FJ (2003). Liver-specific disruption of PPARgamma in leptin-deficient mice improves fatty liver but aggravates diabetic phenotypes. J Clin Invest 111, 737–747. [PubMed: 12618528]

Matz-Soja M, Rennert C, Schonefeld K, Aleithe S, Boettger J, Schmidt-Heck W, Weiss TS, Hovhannisyan A, Zellmer S, Kloting N, et al. (2016). Hedgehog signaling is a potent regulator of liver lipid metabolism and reveals a GLI-code associated with steatosis. Elife 5.

Mercer TR, Dinger ME, and Mattick JS (2009). Long non-coding RNAs: insights into functions. Nature Reviews Genetics 10, 155–159.

Morris KV, and Mattick JS (2014). The rise of regulatory RNA. Nat Rev Genet 15, 423–437. [PubMed: 24776770]

Ponting CP, Oliver PL, and Reik W (2009). Evolution and functions of long noncoding RNAs. Cell 136, 629–641. [PubMed: 19239885]

Pospisilik JA, Schramek D, Schnidar H, Cronin SJ, Nehme NT, Zhang X, Knauf C, Cani PD, Aumayr K, Todoric J, et al. (2010). Drosophila genome-wide obesity screen reveals hedgehog as a determinant of brown versus white adipose cell fate. Cell 140, 148–160. [PubMed: 20074523]

Prasanth KV, and Spector DL (2007). Eukaryotic regulatory RNAs: an answer to the 'genome complexity' conundrum. Genes Dev 21, 11–42. [PubMed: 17210785]

Quinn JJ, and Chang HY (2016). Unique features of long non-coding RNA biogenesis and function. Nat Rev Genet 17, 47–62. [PubMed: 26666209]

Ran FA, Hsu PD, Wright J, Agarwala V, Scott DA, and Zhang F (2013). Genome engineering using the CRISPR-Cas9 system. Nat Protoc 8, 2281–2308. [PubMed: 24157548]

Regue L, Minichiello L, Avruch J, and Dai N (2019). Liver-specific deletion of IGF2 mRNA binding protein-2/IMP2 reduces hepatic fatty acid oxidation and increases hepatic triglyceride accumulation. J Biol Chem 294, 11944–11951. [PubMed: 31209109]

Rinn JL, and Chang HY (2012). Genome regulation by long noncoding RNAs. Annu Rev Biochem 81, 145–166. [PubMed: 22663078]

Rubin LL, and de Sauvage FJ (2006). Targeting the Hedgehog pathway in cancer. Nat Rev Drug Discov 5, 1026–1033. [PubMed: 17139287]

Schmidt-Heck W, Matz-Soja M, Aleithe S, Marbach E, Guthke R, and Gebhardt R (2015). Fuzzy modeling reveals a dynamic self-sustaining network of the GLI transcription factors controlling important metabolic regulators in adult mouse hepatocytes. Molecular bioSystems 11, 2190–2197. [PubMed: 26010061]

Semple RK, Chatterjee VK, and O'Rahilly S (2006). PPAR gamma and human metabolic disease. J Clin Invest 116, 581–589. [PubMed: 16511590]

Suh JM, Gao X, McKay J, McKay R, Salo Z, and Graff JM (2006). Hedgehog signaling plays a conserved role in inhibiting fat formation. Cell Metab 3, 25–34. [PubMed: 16399502]

Swiderska-Syn M, Suzuki A, Guy CD, Schwimmer JB, Abdelmalek MF, Lavine JE, and Diehl AM (2013). Hedgehog pathway and pediatric nonalcoholic fatty liver disease. Hepatology 57, 1814–1825. [PubMed: 23300059]

Teperino R, Amann S, Bayer M, McGee SL, Loipetzberger A, Connor T, Jaeger C, Kammerer B, Winter L, Wiche G, et al. (2012). Hedgehog partial agonism drives Warburg-like metabolism in muscle and brown fat. Cell 151, 414–426. [PubMed: 23063129]

Todoric J, Strobl B, Jais A, Boucheron N, Bayer M, Amann S, Lindroos J, Teperino R, Prager G, Bilban M, et al. (2011). Cross-talk between interferon-γ and hedgehog signaling regulates adipogenesis. Diabetes 60, 1668–1676. [PubMed: 21536945]

Tybl E, Shi FD, Kessler SM, Tierling S, Walter J, Bohle RM, Wieland S, Zhang J, Tan EM, and Kiemer AK (2011). Overexpression of the IGF2-mRNA binding protein p62 in transgenic mice induces a steatotic phenotype. J Hepatol 54, 994–1001. [PubMed: 21145819]

Ulitsky I, and Bartel DP (2013). lincRNAs: genomics, evolution, and mechanisms. Cell 154, 26–46. [PubMed: 23827673]

Venteclef N, Jakobsson T, Steffensen KR, and Treuter E (2011). Metabolic nuclear receptor signaling and the inflammatory acute phase response. Trends Endocrinol Metab 22, 333–343. [PubMed: 21646028]

Vidal-Puig A, Jimenez-Liñan M, Lowell BB, Hamann A, Hu E, Spiegelman B, Flier JS, and Moller DE (1996). Regulation of PPAR gamma gene expression by nutrition and obesity in rodents. The Journal of Clinical Investigation 97, 2553–2561. [PubMed: 8647948]

Vokes SA, Ji H, McCuine S, Tenzen T, Giles S, Zhong S, Longabaugh WJ, Davidson EH, Wong WH, and McMahon AP (2007). Genomic characterization of Gli-activator targets in sonic hedgehog-mediated neural patterning. Development 134, 1977–1989. [PubMed: 17442700]

Vokes SA, Ji H, Wong WH, and McMahon AP (2008). A genome-scale analysis of the cis-regulatory circuitry underlying sonic hedgehog-mediated patterning of the mammalian limb. Genes Dev 22, 2651–2663. [PubMed: 18832070]

Wang L, Park HJ, Dasari S, Wang S, Kocher JP, and Li W (2013). CPAT: Coding-Potential Assessment Tool using an alignment-free logistic regression model. Nucleic Acids Res 41, e74. [PubMed: 23335781]

Wu J, Zhu P, Lu T, Du Y, Wang Y, He L, Ye B, Liu B, Yang L, Wang J, et al. (2019). The long non-coding RNA LncHDAC2 drives the self-renewal of liver cancer stem cells via activation of Hedgehog signaling. J Hepatol 70, 918–929. [PubMed: 30582981]

Xing Z, Lin A, Li C, Liang K, Wang S, Liu Y, Park PK, Qin L, Wei Y, Hawke DH, et al. (2014). lncRNA directs cooperative epigenetic regulation downstream of chemokine signals. Cell 159, 1110–1125. [PubMed: 25416949]

Yang H, Wang H, and Jaenisch R (2014). Generating genetically modified mice using CRISPR/Cas-mediated genome engineering. Nat Protoc 9, 1956–1968. [PubMed: 25058643]

Yao Q, Liu J, Xiao L, and Wang N (2019a). Sonic hedgehog signaling instigates high-fat diet-induced insulin resistance by targeting PPARgamma stability. J Biol Chem 294, 3284–3293. [PubMed: 30573683]

Yao RW, Wang Y, and Chen LL (2019b). Cellular functions of long noncoding RNAs. Nat Cell Biol 21, 542–551. [PubMed: 31048766]

Zhou H, Xiong Y, Peng L, Wang R, Zhang H, and Fu Z (2020). LncRNA-cCSC1 modulates cancer stem cell properties in colorectal cancer via activation of the Hedgehog signaling pathway. J Cell Biochem 121, 2510–2524. [PubMed: 31680315]

Zhou M, Hou Y, Yang G, Zhang H, Tu G, Du YE, Wen S, Xu L, Tang X, Tang S, et al. (2016). LncRNA-Hh Strengthen Cancer Stem Cells Generation in Twist-Positive Breast Cancer via Activation of Hedgehog Signaling Pathway. Stem Cells 34, 55–66. [PubMed: 26418365]

Highlights

Hilnc is directly regulated by Hh signaling *in vitro* and *in vivo*

Hilnc$^{BM/BM}$ and *Hilnc*$^{-/-}$ mice are resistant to diet-induced obesity and fatty liver

Lack of *Hilnc* decreases lipid accumulation in primary hepatocytes and prevents diet-induced hepatic steatosis

Hilnc binds to IGF2BP2 to regulate the mRNA stability of *Pparγ*

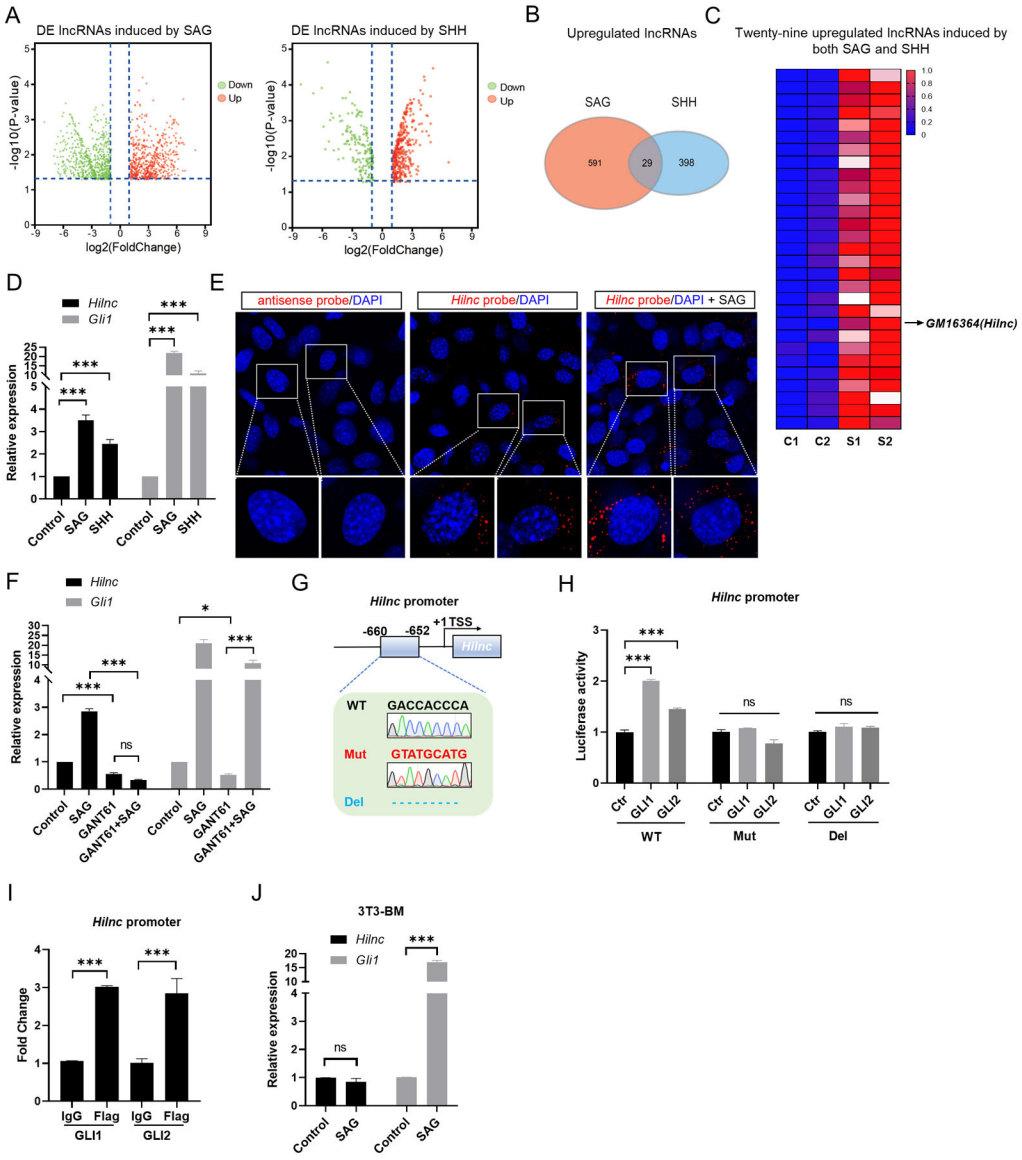

Figure 1. Identification of *GM16364* as a lncRNA (*Hilnc*) that is directly induced by Hedgehog signaling.

(A) Volcano plot showing lncRNAs that were differentially expressed (DE) in NIH-3T3 cells after treatment with SAG (200 nM, left) and SHH (1 μg/ml, right) for 24 hours, as determined by RNA-seq.

(B) Venn diagram of lncRNAs that were upregulated in NIH-3T3 cells after treatment with SAG and SHH.

(C) Heatmap representation of 29 example lncRNAs (fold change > 2; FDR-adjusted P < 0.05) that were upregulated in NIH-3T3 cells after treatment with SAG and SHH. The arrow indicates *GM16364 (Hilnc)*. The heatmap is draw based on normalized expression levels.

(D) Relative expression of *Hilnc* and *Gli1* after SAG and SHH treatment in NIH-3T3 cells. Expression levels were normalized to 18s RNA.

(E) RNA FISH for *Hilnc* in NIH-3T3 cells showed that *Hilnc* mostly resided in the cytoplasm and that SAG treatment upregulated *Hilnc* expression in NIH-3T3 cells. A DIG-

labeled sense full-length *Hilnc* transcript was used as an RNA probe, and a DIG-labeled antisense *Hilnc* transcript was used as a control. RNA signals are shown in red, and DAPI staining is shown in blue.

(F) Relative expression of *Hilnc* and *Gli1* after treatment with SAG, GANT61 (10 μM) or both SAG and GANT61 in NIH-3T3 cells.

(G) Schematic diagram of the *Hilnc* promoter region with a conserved Gli binding site (WT), randomly mutated Gli binding site (Mut) and deleted Gli binding site (Del).

(H) A luciferase reporter driven by the WT or mutated/deleted *Hilnc* promoter (as shown in G) was transfected in the presence or absence of Gli1 and Gli2.

(I) Chromatin immunoprecipitation (ChIP) analysis showed the binding of Gli1/Gli2 to the *Hilnc* promoter. NIH-3T3 cells were transfected with Flag-Gli1/Flag-Gli2 for 24 hours. Protein-bound chromatin was immunoprecipitated with the anti-Flag antibody, and IgG was used as a control. The immunoprecipitated DNA was analyzed by quantitative PCR (qPCR) using primers targeting the *Hilnc* promoter.

(J) Relative expression of *Hilnc* and *Gli1* after SAG treatment in 3T3-BM (the Gli binding site mutant) cells.

The data in D, F, H, I and J represent the mean ± SEM. Unpaired t tests and one-way ANOVA were used to compare the differences between groups. *P < 0.05, ***P < 0.001, ns means not significant.

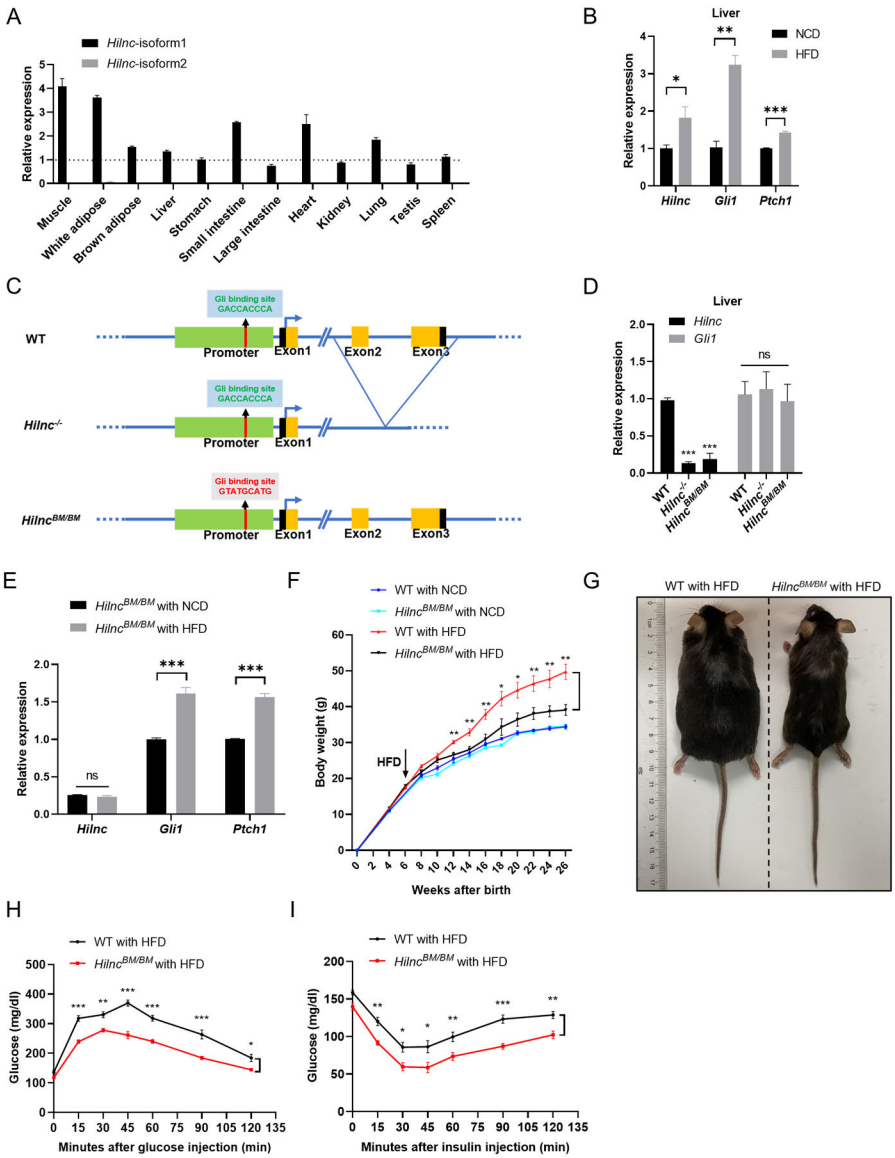

Figure 2. Gli1 directly regulates the expression of *Hilnc in vivo*, and *Hilnc*$^{BM/BM}$ mice are resistant to diet-induced obesity.

(A) Relative expression of two isoforms of *Hilnc* in different mouse tissues was measured by qPCR.

(B) Relative expression of *Hilnc*, *Gli1* and *Ptch1* in the livers of 22-week-old WT mice fed a NCD or HFD for 16 weeks. Expression levels were normalized to the 18s RNA level.

(C) Generation of *Hilnc*$^{-/-}$ and *Hilnc*$^{BM/BM}$ mice.

(D) Relative expression of *Hilnc* and *Gli1* in the livers of WT, *Hilnc*$^{-/-}$ and *Hilnc*$^{BM/BM}$ mice.

(E) Relative expression of *Hilnc*, *Gli1* and *Ptch1* in the livers of 22-week-old *Hilnc*$^{BM/BM}$ mice fed a NCD or HFD for 16 weeks.

(F) Growth curves of WT and *Hilnc*$^{BM/BM}$ mice on NCD and HFD, respectively. The body weights of WT and *Hilnc*$^{BM/BM}$ mice fed a NCD were not different at any age. WT and *Hilnc*$^{BM/BM}$ mice were fed a HFD from 6 weeks of age (indicated by the arrow); their

weights were not different at 6 weeks, but the weights of WT mice were significantly greater from 12 weeks of age ($p < 0.05$) and thereafter (n=5).

(G) Representative images of 22-week-old WT and *Hilnc*$^{BM/BM}$ male mice fed a HFD for 16 weeks.

(H) Glucose tolerance tests. Glucose, 1 g/kg, was administered intraperitoneally after 14 hours of fasting in 12-week-old WT or *Hilnc*$^{BM/BM}$ male mice fed a HFD for 6 weeks (n=6).

(I) Insulin tolerance tests. Insulin, 0.4 U/kg, was administered intraperitoneally after 5 hours of fasting in 12-week-old WT or *Hilnc*$^{BM/BM}$ male mice fed a HFD for 6 weeks (n=6).

The data in A, B, D, E, F, H and I represent the mean ± SEM. Unpaired t tests and one-way ANOVA were used to compare the differences between groups. *P < 0.05, **P < 0.01, ***P < 0.001, ns means not significant.

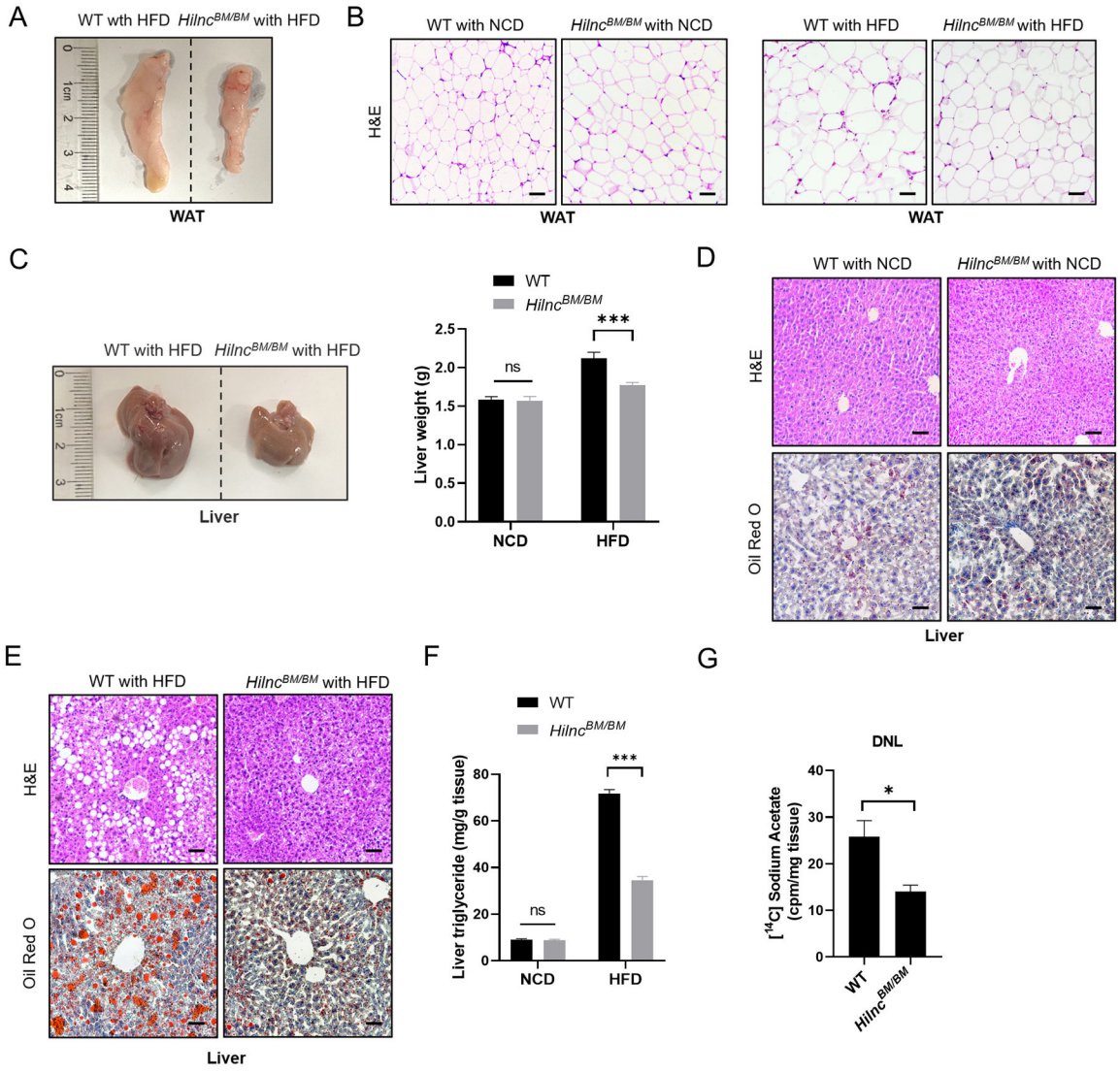

Figure 3. *Hilnc*$^{BM/BM}$ mice are resistant to diet-induced obesity and fatty liver.

(A) Representative images of abdominal WAT of 22-week-old WT and *Hilnc*$^{BM/BM}$ mice fed a HFD for 16 weeks.

(B) H&E staining of abdominal WAT of 22-week-old WT and *Hilnc*$^{BM/BM}$ mice fed a NCD (left) and HFD (right) for 16 weeks; scale bar, 50 μm.

(C) Representative images of a liver (left) and liver weights (right, n=5) of 22-week-old WT and *Hilnc*$^{BM/BM}$ mice fed a HFD for 16 weeks.

(D) (E) H&E and oil Red O staining of liver sections from 22-week-old WT and *Hilnc*$^{BM/BM}$ mice fed a NCD (D) or HFD (E) for 16 weeks; scale bar, 50 μm.

(F) The hepatic TG levels of 22-week-old WT and *Hilnc*$^{BM/BM}$ mice fed a NCD or HFD were determined (n=6).

(G) De novo lipogenesis (DNL) activity of liver from WT and *Hilnc*$^{BM/BM}$ mice.

The data in C, F and G represent the mean ± SEM. Unpaired t tests and one-way ANOVA were used to compare the differences between groups. ***P < 0.001, ns means not significant.

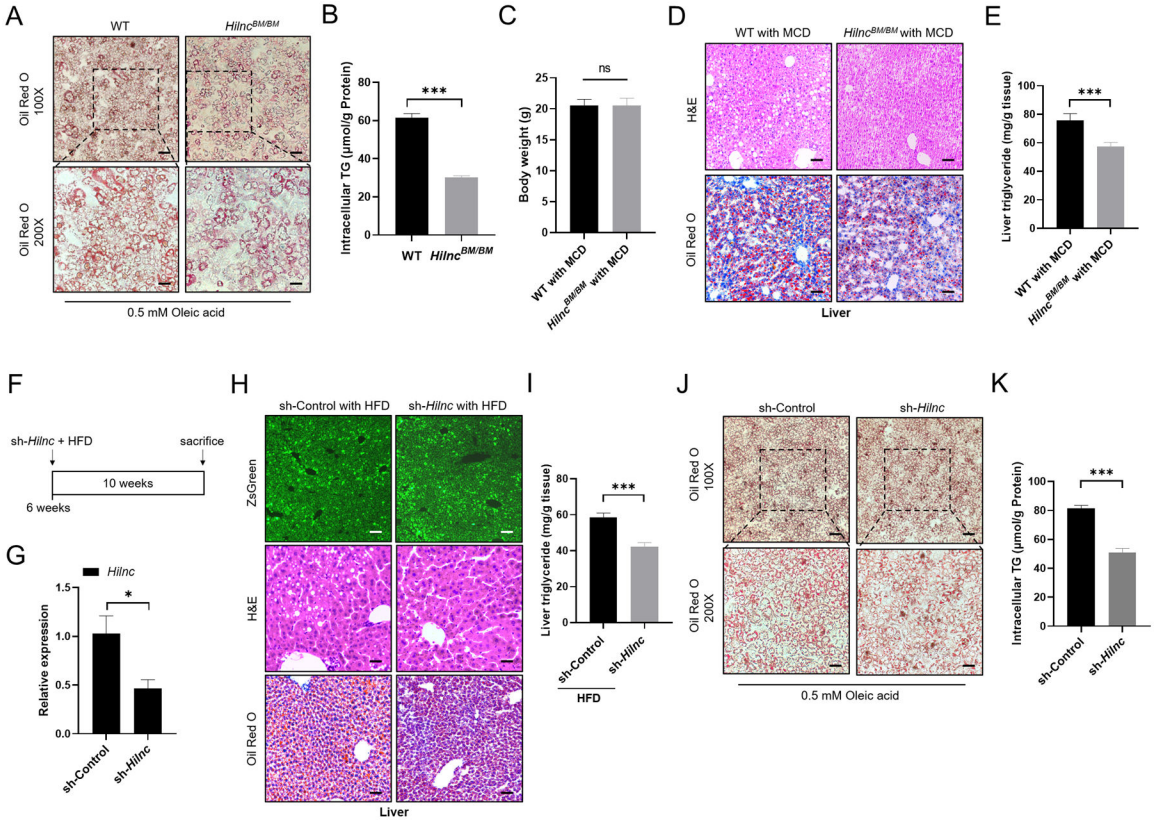

Figure 4. Lack of *Hilnc* decreases lipid accumulation in primary hepatocytes and prevents diet-induced hepatic steatosis.

(A) Oil Red O staining of primary hepatocytes isolated from WT and *Hilnc*$^{BM/BM}$ mice after 0.5 mM oleic acid (OA) treatment; scale bar, 100 μm (upper), 50 μm (lower).

(B) Intracellular TG levels of primary hepatocytes isolated from WT and *Hilnc*$^{BM/BM}$ mice after OA treatment.

(C) Body weights of 12-week-old WT and *Hilnc*$^{BM/BM}$ male mice fed a MCD for one month (n=5).

(D) H&E and oil Red O staining of liver sections from 12-week-old WT and *Hilnc*$^{BM/BM}$ mice fed a MCD for 1 month; scale bar, 50 μm.

(E) The hepatic TG levels of 12-week-old WT and *Hilnc*$^{BM/BM}$ male mice fed a MCD for 1 month were determined (n=5).

(F) Six-week-old WT male mice were injected with adenoviral sh-Control or sh-*Hilnc* via the tail vein. After 10 weeks of continuous HFD feeding, the mice were sacrificed.

(G) qPCR analysis showed efficient knockdown of *Hilnc* in mouse livers.

(H) Immunofluorescence (ZsGreen), H&E and oil Red O staining of liver sections from control and *Hilnc*-knockdown mice fed a HFD; scale bar, 100 μm (upper), 50 μm (middle and lower).

(I) The hepatic TG levels of control and *Hilnc*-knockdown mice fed a HFD were determined (n=5).

(J) Oil Red O staining of primary hepatocytes isolated from control or *Hilnc*-knockdown mice after OA treatment; scale bar, 100 μm (upper), 50 μm (lower).

(K) Intracellular TG levels of primary hepatocytes isolated from control and *Hilnc*-knockdown mice after OA treatment.

The data in B, C, E, G, I and K represent the mean ± SEM. Unpaired t tests and one-way ANOVA were used to compare the differences between groups. *P < 0.05, ***P < 0.001, ns means not significant.

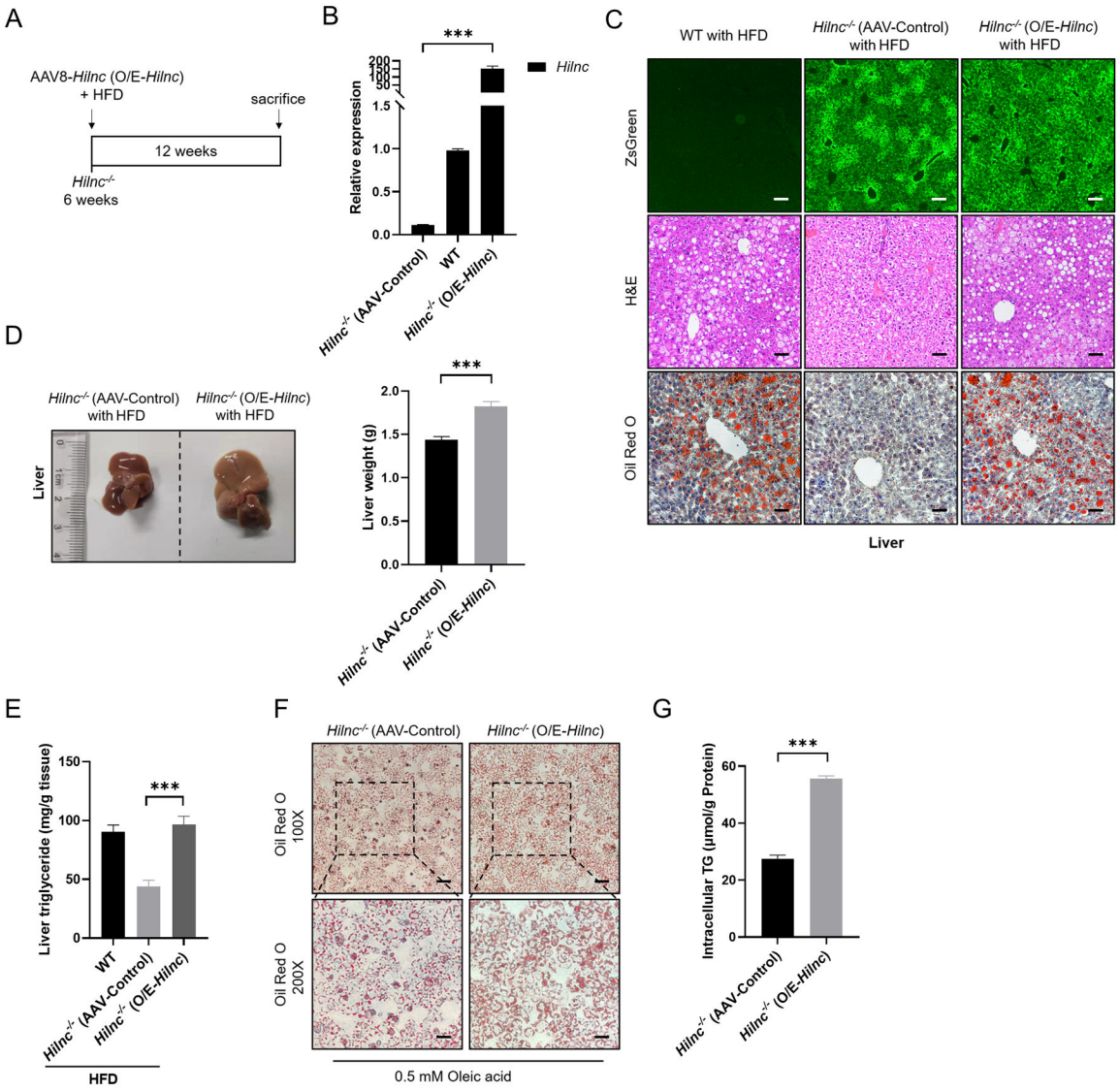

Figure 5. Overexpression of *Hilnc* in the liver of *Hilnc*$^{-/-}$ mice results in increased lipid accumulation.

(A) *Hilnc*$^{-/-}$ mice at 6 weeks of age were injected with AAV8-GFP (AAV-Control) or AAV8-*Hilnc* (O/E-*Hilnc*). After 12 weeks of continuous HFD feeding, the mice were sacrificed.

(B) qPCR analysis showed successful overexpression of *Hilnc* in *Hilnc*$^{-/-}$ mouse livers.

(C) Immunofluorescence (ZsGreen), H&E and oil Red O staining of liver sections from WT, *Hilnc*$^{-/-}$ (AAV-Control) and *Hilnc*$^{-/-}$ (O/E-*Hilnc*) mice fed a HFD; scale bar, 200 μm (upper), 50 μm (middle and lower).

(D) Representative images of the liver (left) and liver weights (right, n=5) of *Hilnc*$^{-/-}$ (AAV-Control) or *Hilnc*$^{-/-}$ (O/E-*Hilnc*) mice fed a HFD.

(E) Hepatic TG levels in the livers of WT, *Hilnc*$^{-/-}$ (AAV-Control) and *Hilnc*$^{-/-}$(O/E-*Hilnc*) mice fed a HFD (n=5).

(F) Oil Red O staining of primary hepatocytes isolated from *Hilnc*$^{-/-}$ (AAV-Control) and *Hilnc*$^{-/-}$ (O/E-*Hilnc*) mice after OA treatment; scale bar, 100 μm (upper), 50 μm (lower).

(G) Intracellular TG levels of primary hepatocytes isolated from *Hilnc*$^{-/-}$ (AAV-Control) and *Hilnc*$^{-/-}$ (O/E-*Hilnc*) mice after OA treatment.

The data in B, D, E and G represent the mean ± SEM. Unpaired t tests and one-way ANOVA were used to compare the differences between groups. ***P < 0.001.

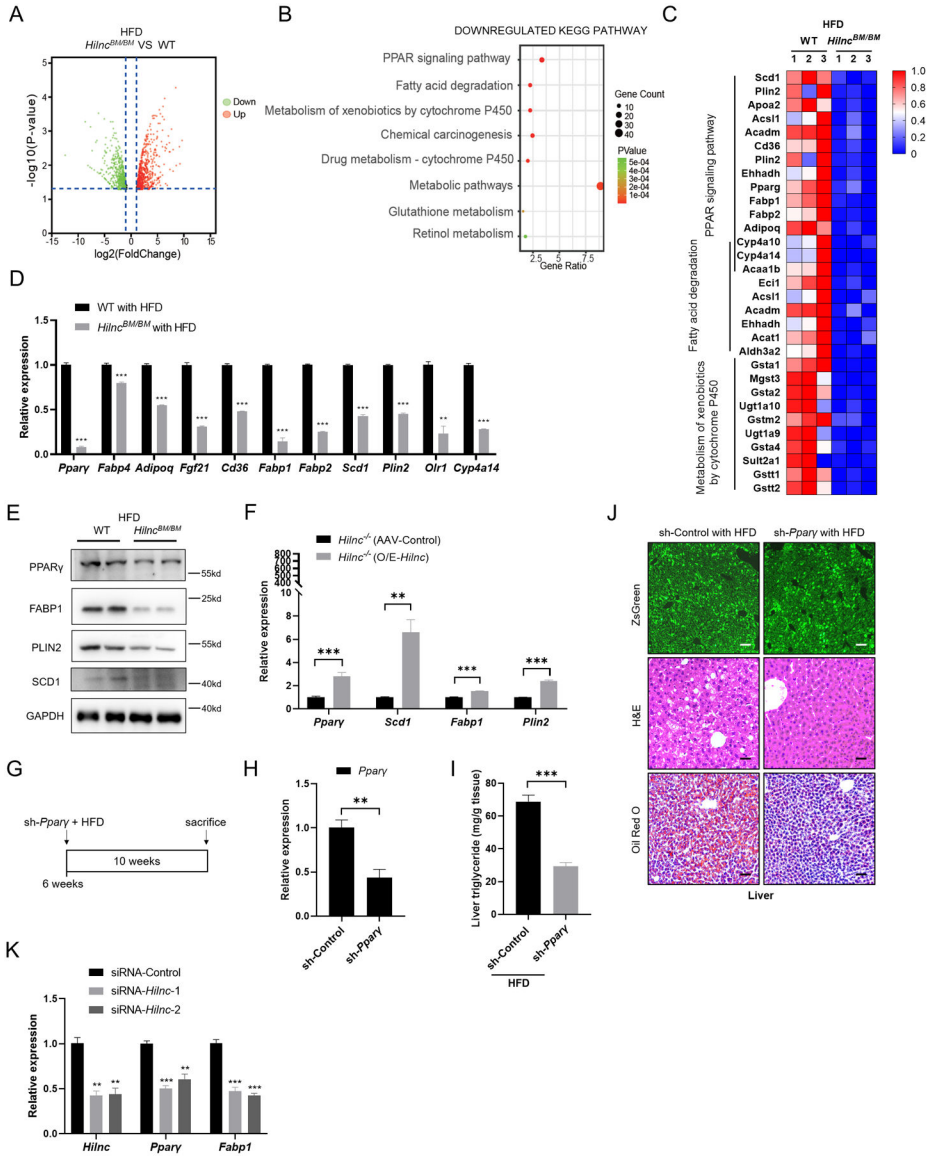

Figure 6. *Hilnc* modulates the PPAR signaling pathway in the liver.

(A) Volcano plot showing the changed genes in the livers of 22-week-old *Hilnc*$^{BM/BM}$ mice fed a HFD for 16 weeks compared with WT livers, as determined by RNA-seq.

(B) Downregulated KEGG pathway enrichment analysis of transcripts that were differentially expressed between livers isolated from WT and *Hilnc*$^{BM/BM}$ mice fed a HFD.

(C) Heat map showing the changed genes that were enriched in different downregulated KEGG pathways.

(D) (E) qPCR (D) and western blot (E) analyses verified the decrease in the changed genes in the PPAR signaling pathway between WT and *Hilnc*$^{BM/BM}$ mice after HFD feeding for 16 weeks.

(F) Overexpression of *Hilnc* in *Hilnc*$^{-/-}$ livers restored the expression of *Pparγ* and other target genes.

(G) Six-week-old WT male mice were injected with adenoviral sh-Control or sh-*Pparγ* via the tail vein. After 10 weeks of continuous HFD feeding, the mice were sacrificed.
(H) qPCR analysis showed efficient knockdown of *Pparγ* in the liver.
(I) Hepatic TG levels of control and *Pparγ*-knockdown mice fed a HFD (n=5).
(J) Immunofluorescence (ZsGreen), H&E and oil Red O staining of liver sections from control and *Pparγ*-knockdown mice after HFD feeding; scale bar, 100 μm (upper), 50 μm (middle and lower).
(K) The mRNA levels of *Pparγ* and *Fabp1* in control and siRNA-mediated *Hilnc*-knockdown AML12 cells treated with OA.
The data in D, F, H, I and K represent the mean ± SEM. Unpaired t tests and one-way ANOVA were used to compare the differences between groups. **P < 0.01, ***P < 0.001, ns means not significant.

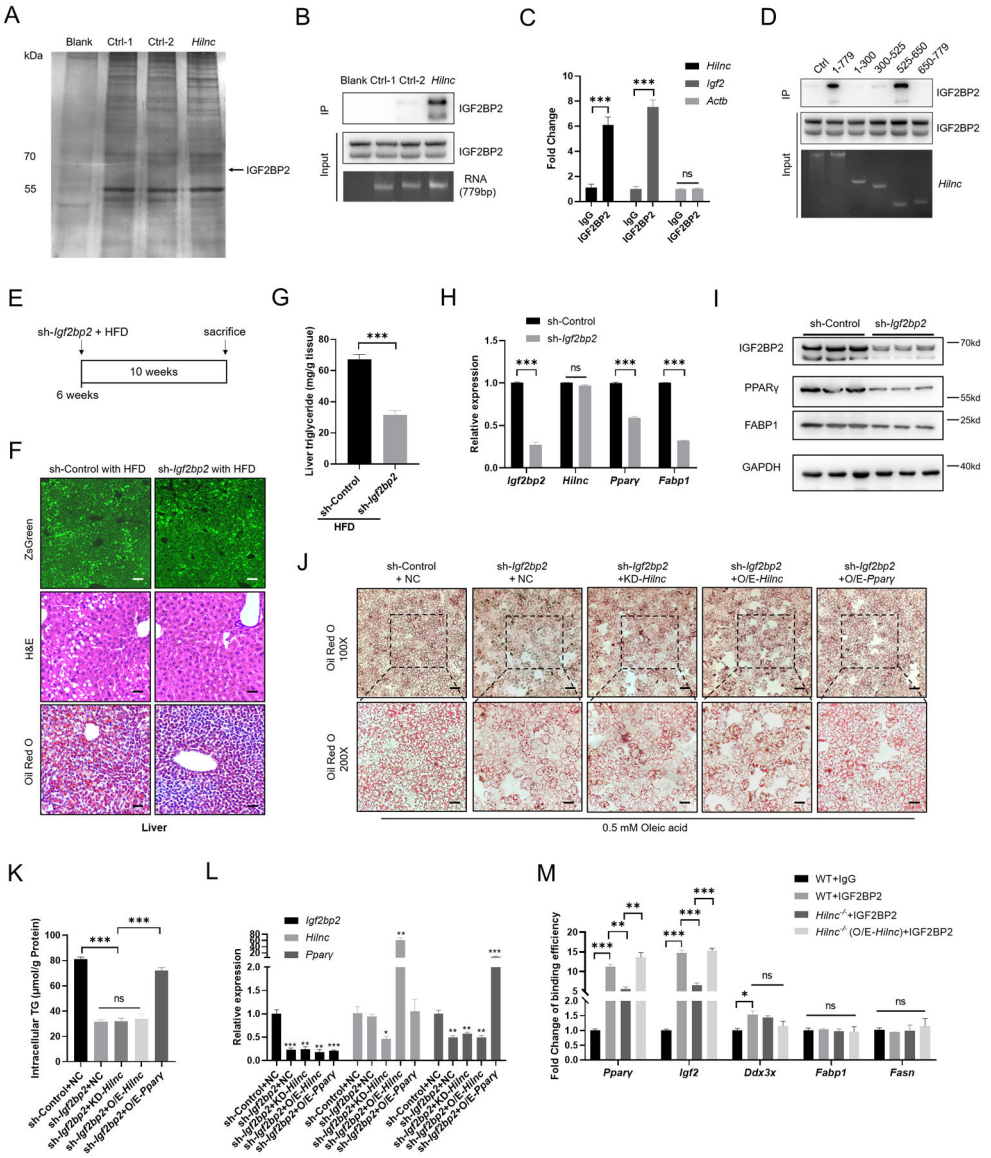

Figure 7. *Hilnc* directly binds to IGF2BP2 and functions through IGF2BP2.

(A) IGF2BP2 is a candidate interaction partner of *Hilnc*. Biotin-labeled sense *Hilnc*, a blank control (blank), an intron control (Ctr-1) and anti-sense *Hilnc* (Ctr-2) were incubated with AML12 cell lysates, and the enriched products were eluted and separated by SDS-PAGE and silver staining. The differential band appearing in the *Hilnc* lane was analyzed by mass spectrometry. The arrow indicates IGF2BP2.

(B) *Hilnc* associated with IGF2BP2, as shown by RNA pulldown and western blot analysis. Biotin-labeled *Hilnc* and controls, including the intron control (Ctr-1) and anti-sense *Hilnc* (Ctr-2), were added to AML12 cell lysates, and pulldown assays were performed.

(C) *Hilnc* was enriched by IGF2BP2 in AML12 cell lysates. The mRNA of Igf2 was employed as a positive control and the mRNA of *Actb* was employed as a negative control.

(D) The 525~650 nt region in *Hilnc* is important for its interaction with IGF2BP2.

(E) Six-week-old WT male mice were injected with adenoviral sh-Control or sh-*Igf2bp2* via the tail vein. After 10 weeks of continuous HFD feeding, the mice were sacrificed.
(F) Immunofluorescence (ZsGreen), H&E and oil Red O staining of liver sections from control and *Igf2bp2*-knockdown mice fed a HFD; scale bar, 100 μm (upper), 50 μm (middle and lower).
(G) Hepatic TG levels in livers from control and *Igf2bp2*-knockdown mice fed a HFD (n=5).
(H) (I) Expression levels of the *Igf2bp2*, *Hilnc*, *Pparγ*, and *Pparγ* downstream gene *Fabp1* in the control and *Igf2bp2*-knockdown mouse livers.
(J) Oil Red O staining of primary hepatocytes isolated from control or *Igf2bp2*-knockdown mouse livers treated with OA after transfection with empty plasmid (NC), siRNA-*Hilnc* (KD-*Hilnc*), pcDNA3.1-*Hilnc* (O/E-*Hilnc*), or pcDNA3.1-Flag-Pparγ (O/E-*Pparγ*); scale bar, 100 μm (upper) and 50 μm (lower).
(K) Intracellular TG levels of primary hepatocytes isolated from control and *Igf2bp2*-knockdown mouse livers after transfection with the indicated plasmids and OA treatment.
(L) qPCR analysis verified the transfection efficiency in primary hepatocytes isolated from control and *Igf2bp2*-knockdown mouse livers.
(M) Enrichment of IGF2BP2-binding mRNAs in IGF2BP2 RIP samples from the liver lysates of WT mice, $Hilnc^{-/-}$ mice or $Hilnc^{-/-}$ (O/E-*Hilnc*) mice.
The data in C, G, H, K, L and M represent the mean ± SEM. Unpaired t tests and one-way ANOVA were used to compare the differences between groups. *P < 0.05, **P < 0.01, ***P < 0.001, ns means not significant.

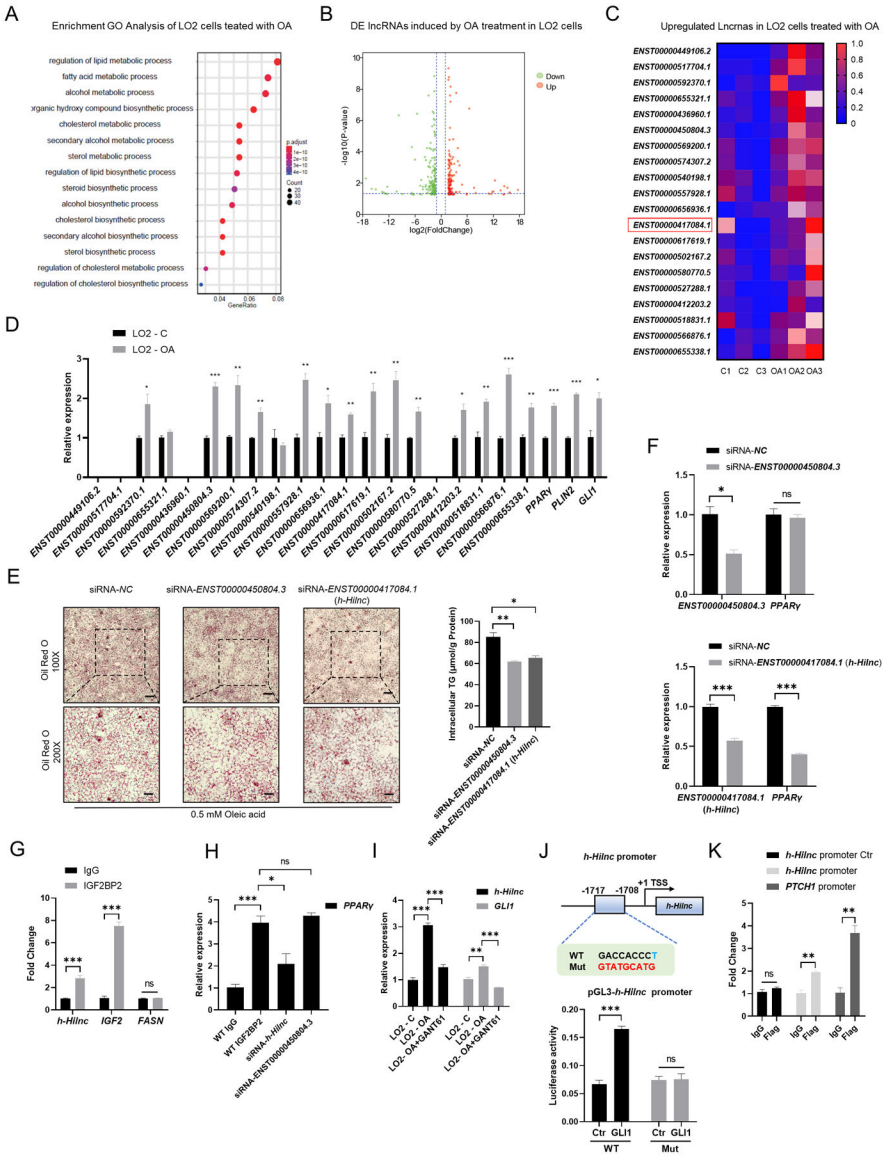

Figure 8. Identification of the potential functional human homolog of *Hilnc*

(A) Enrichment GO Analysis of LO2 cells with OA treatment.

(B) Volcano plot showing the changed genes in the LO2 cells with OA treatment, as determined by RNA-seq.

(C) Heat map showing the 20 upregulated lncRNAs that had predicted Gli binding sites near their TSS. The heatmap is draw based on normalized expression levels.

(D) qPCR analysis showing the upregulation of 14 lncRNAs and the upregulation of *PPARγ*, *PLIN2* and *GLI1* in LO2 cells with OA treatment.

(E) Oil Red O staining and Intracellular TG measurement showed that knocking down *ENST00000450804.3* and *ENST00000417084.1* decreased lipid accumulation of LO2 cells treated with OA; scale bar, 100 μm (upper), 50 μm (lower).

(F) qPCR analysis showing the knocking down efficiency of *ENST00000450804.3* and *ENST00000417084.1* and the relative expression level of *PPARγ*.

(G) *h-Hilnc* was enriched by IGF2BP2 in LO2 cell lysates. The mRNA of *IGF2* was employed as a positive control and the mRNA of *FASN* was employed as a negative control.
(H) Knocking down *h-Hilnc* decreased the binding of IGF2BP2 to *PPARγ*, while knocking down *ENST00000450804.3* didn't.
(I) GANT61 decreased the expression of *h-Hilnc* and *GLI1* in LO2 cells with OA treatment.
(J) A luciferase reporter driven by the WT or mutated *h-Hilnc* promoter was transfected in the presence or absence of GLI1.
(K) ChIP analysis showed the binding of GLI1 to the *h-Hilnc* promoter. LO2 cells were transfected with Flag-GLI1 for 24 hours. Protein-bound chromatin was immunoprecipitated with the anti-Flag antibody, and IgG was used as a control. The immunoprecipitated DNA was analyzed by qPCR using primers targeting the *PTCH1* promoter with the Gli binding site (*PTCH1* promoter), the *h-Hilnc* promoter with the Gli binding site (*h-Hilnc* promoter) and the *h-Hilnc* promoter without the Gli binding site (*h-Hilnc* promoter Ctr).
The data in D, E, F, G, H, I, J and K represent the mean ± SEM. Unpaired t tests and one-way ANOVA were used to compare the differences between groups. *P < 0.05, **P < 0.01, ***P < 0.001, ns means not significant.